UNITED NATIONS EDUCATIONAL, SCIENTIFIC AND CULTURAL ORGANIZATION
INTERNATIONAL ATOMIC ENERGY AGENCY
INTERNATIONAL CENTRE FOR THEORETICAL PHYSICS
I.C.T.P., P.O. BOX 586, 34100 TRIESTE, ITALY, CABLE: CENTRATOM TRIESTE

H4.SMR/1013-18

SCHOOL ON THE USE OF SYNCHROTRON RADIATION
IN SCIENCE AND TECHNOLOGY:
*"John Fuggle Memorial"*

3 November - 5 December 1997

*Miramare - Trieste, Italy*

---

# *High-Resolution Core-Level Photoelectron Spectroscopy of Surfaces and Adsorbates*

**A. Nilsson**
**University of Uppsala**
**Sweden**

# 3. High-Resolution Core-Level Photoelectron Spectroscopy of Surfaces and Adsorbates

*N. Mårtensson* and *A. Nilsson*

In the present chapter we will discuss some general aspects of core-level photoelectron spectroscopy for the investigation of surfaces and adsorbates. We will focus on a few aspects of this spectroscopy. In Sect. 3.2 some experimental comments will be given of a general nature and referring to the systems which have been used in most of the studies reviewed in this contribution. Sections 3.3–5 deal with core-level shifts, Section 3.3 gives a general introduction and discusses the role of initial and final state effects, Section 3.4 treats shifts of adsorbate lines, and Sect. 3.5 deals with surface core-level shifts for metals. Section 3.6–8 discuss core-level line shapes and core-level satellites. In Sect. 3.6 the most important contributions to the line shape are reviewed. Section 3.7 discusses vibrational broadening, and Sect. 3.8 then deals with shake-up satellites for adsorbates.

## 3.1 Background

Photoelectron spectroscopy can be used to investigate a variety of properties of surfaces, and adsorbed atoms and molecules [3.1–9]. Photoelectron spectroscopy provides direct information on the electronic states in a system. This chapter will focus on the investigation of core electrons, i.e. the electrons which are localized on a particular atomic site and which do not take part in chemical bonding.

There are a number of core-level spectroscopies which are used for the investigation of solids and surfaces. The most important of these are schematically reproduced in Fig. 3.1. The figure shows the valence and core levels for one of the atoms in a system. In core-level photoelectron spectroscopy (Fig. 3.1a), a photon (with energy $h\upsilon$) is absorbed by the system which emits a core electron. Its kinetic energy $E_{kin}$ is given by

$$E_{kin} = h\upsilon - E_B - \phi, \tag{3.1}$$

where $\phi$ is the sample work function (this requires that the kinetic energy just outside the sample is considered. If $E_{kin}$ denotes the kinetic energy in the spectrometer, $\phi$ is instead the work function of the spectrometer). $E_B$ denotes the binding energy of the core electron relative to the Fermi level. In order to excite

Springer Series in Surface Sciences, Vol. 35
Applications of Synchrotron Radiation Ed.: W. Eberhardt

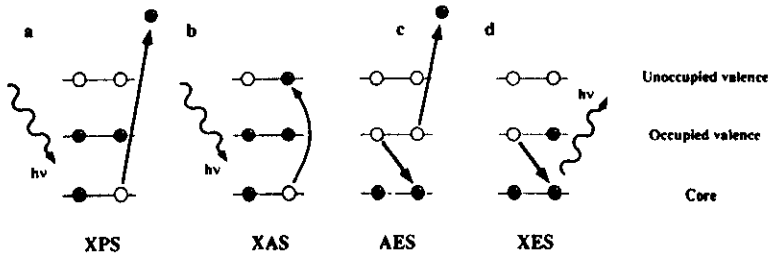


**Fig. 3.1a-d.** A schematic illustration of core level ionization, excitation and decay processes

a core electron, X-ray photons have to be used. The technique is referred to as XPS (X-ray Photoelectron Spectroscopy) or ESCA (Electron Spectroscopy for Chemical Analysis).

Figure 3.1b represents an X-ray absorption process where a core electron is excited to an initially empty valence orbital. The measurements are made by recording the absorption as a function of photon energy at and above the core-level threshold. This requires a tuneable photon source and is usually performed using synchrotron radiation. X-ray Absorption Spectroscopy (XAS) provides a method to study the empty valence-electron states of a system [3.10, 11]. When this method is used for surfaces it is often referred to as NEXAFS (Near Edge X-ray Absorption Fine Structure) [3.10].

Figures 3.1c and 3.1d depict the two types of processes by which a core ionized atom decays. For light elements and shallow core levels the Auger process dominates (Fig. 3.1c). The core hole is filled by an electron from one of the outer shells and the excess energy is taken up by an electron which is emitted from the system. For heavier elements and for deeper core levels the decay is instead dominated by X-ray emission processes (see Fig. 3.1d) in which the excess energy is emitted in the form of a photon. For all core levels both types of processes contribute. The added rates of these decay channels determine the life time of the core hole state and thereby the intrinsic width of the core electron line. The analysis of the emitted electrons or photons is the basis for Auger Electron Spectroscopy (AES) [3.12, 13] or X-ray Emission Spectroscopy (XES) [3.14], respectively. X-ray emission spectroscopy is traditionally a bulk technique but it has recently been shown that it can also be used to investigate the electronic structure of adsorbates [3.15]. The neutral core-excited XAS final states will decay by corresponding processes. The analogue of the Auger process is then denoted autoionization (Chap. 6).

The present chapter will almost entirely deal with photoelectron spectroscopy, although the relationship to the other spectroscopies will be mentioned in some cases. Each element in the periodic table has a unique pattern of core-level binding energies. This makes all core-level spectroscopies sensitive to what elements are present in a sample. A particularly useful property of XPS is that



the detailed core-level positions depend on the chemical state of the probed atoms (chemical shifts). The chemical shifts can be used as fingerprints of different adsorbate species, such as for instance to monitor the dissociation of a molecular adsorbate. By analyzing the shifts within the framework of various theoretical models, it is possible to extract basic information on the electronic structure of the adsorbate complex as well as information of a thermochemical nature. This often requires rather elaborate theoretical considerations which, for instance, take into account the response of the complete system to the creation of the core hole (screening or relaxation). By combining photoelectron spectroscopy with other core-level spectroscopies, additional information can be obtained on matters like the dynamics of core-hole screening, vibrational interference, etc.

One of the important properties of core-level spectroscopies is that the core hole is localized at one atom. In this way all core-level spectroscopies probe local aspects of the sample. For instance, in the XAS and XES processes the obtained valence-electron information corresponds to a projection of the valence-electron structure on the core hole site. For an adsorbate, this implies that by recording spectra involving the adsorbate core levels, the adsorbate valence states are probed without overlapping contributions from the substrate. This distinguishes core-level spectroscopies from methods like valence band photoemission. In core-level photoemission the emitted electrons also undergo diffraction processes. The core ionized atom then acts as a point source of electrons for the scattering which makes the technique sensitive to the local structure. This is different from a regular electron scattering experiment like LEED (Low Energy Electron Diffraction) where the diffraction of an incoming electron wave is considered. XPD (X-ray Photoelectron Diffraction) is now an established structural technique [3.16]. It will be discussed further in Chap. 4.

Many of the basic properties of photoelectron spectroscopy can be visualized using the spectra in Fig. 3.2. This figure displays a series of Yb $4f$ photoelectron spectra from Yb layers of different thicknesses deposited on a Mo(110) substrate [3.17]. Yb grows in a layer-by-layer fashion and spectra are shown for 1, 2 and 3 MonoLayer (ML) films and for a thick epitaxial Yb layer. The $4f$ photoemission leads to a spin-orbit split $4f_{7/2}/4f_{5/2}$ doublet with an energy separation of 1.27 eV. The intensity ratio is 4/3, which is determined by the degeneracies of the two levels involved. Although the $4f$ level has a very low binding energy it can be treated as a core level. This is due to the small spatial extension of the $4f$ orbitals which implies that it does not take part in the bonding.

When one ML of Yb is deposited the spectrum shows one $4f$ doublet. For the 2 ML film two chemically shifted Yb $4f$ doublets are seen. The shift between these is due to the fact that the atoms in the two layers have different chemical surroundings; the top-most layer is an Yb surface layer with a layer of Yb atoms underneath, i.e., the atoms have the same distribution of nearest neighbours as a surface atom on a thick Yb sample. The atoms in the interface layer are surrounded by both Yb and Mo atoms.

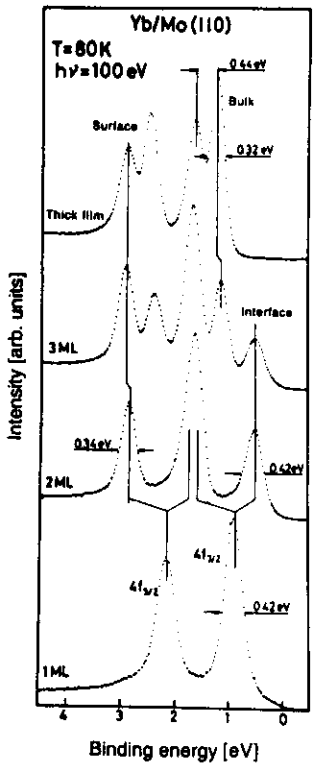


**Fig. 3.2.** Photoelectron spectra, showing the Yb 4*f*-region for different coverages of Yb on Mo(110). At a photon energy of 100 eV, the Yb 4*f* emission dominates totally over the contribution from the Mo substrate

In the 3 ML spectrum three shifted Yb components are seen; the two components in the 2 ML spectrum remain at nearly the same energies and a third component appears at an intermediate energy. The latter feature originates from the middle layer which has a complete nearest neighbour shell of Yb atoms. In a nearest neighbour sense the middle layer already represents a bulk Yb layer. Further depositions only result in intensity changes of these three components [3.18] and no new spectral features appear. Eventually the film gets so thick that the interface peaks are completely attenuated and the upper spectrum of Fig. 3.2, characteristic of a thick Yb film, is obtained.

This example immediately shows that the shifts are dominated by the nearest neighbours. This is seen from the fact that the surface and interface peaks have the same energies for the 2 and 3 ML films and from the fact that the bulk Yb binding energy is almost attained by three monolayers of Yb. This is a most useful property of the chemical shift which makes it possible to draw direct conclusions about the local coordination in a system by measuring core-level spectra. This approach has been described in detail for alloy systems [3.19] and



will be further discussed below for adsorbates. Even if the nearest neighbours dominate the chemical shifts, there are some second-order effects. In the Yb spectra above, the Mo substrate is seen to shift also the second Yb layer by 0.05 eV (7% of the first-order shift). There are, however, cases where the electronic structure may be very sensitive to chemical modifications, which will lead to chemical shift effects that range over a much larger number of coordination shells.

Figure 3.2 also demonstrates the surface sensitivity of the technique. The interface peak is seen in all the situations except the thick film but its intensity is reduced by approximately a factor of two for each additional Yb layer. Hence, for the electron transport through one atomic layer of Yb, about 50% of the electrons undergo inelastic scattering and are lost in the spectrum. This property of the spectra is also seen directly in the 3 ML spectrum for which an intensity ratio of about 1:2:4 is observed for the three layers. For the thick sample almost 50% of the total intensity originates from the top-most atomic layer.

The information depth depends on the kinetic energy of the photoelectrons. The mean-free path as a function of electron energy has a minimum at about 50 eV. The exact position of the minimum, however, depends on the material.

When a core electron is emitted this causes a perturbation of the whole system. This leads to so-called shake-up and shake-off processes [3.20, 1]. Figure 3.3 shows the photoelectron spectrum related to the ionization of the Ne 1*s* level for the free atom [3.21, 22]. The one-electron removal of the 1*s* electron corresponds to the main peak at 870.3 eV [3.23]. However, there are a number of additional spectral features at higher binding energies and a continuum is seen which extends some 100 eV above the main line. The Ne atom has a $1s^2 2s^2 2p^6$ configuration. When a core electron is photoionized this may lead to the excitation of a 2*p* electron to a higher *np* shell. A number of such 2*p*-*np* shake-up peaks are seen in the spectrum. At still higher excitation energies relative to the main line, 2*s*-*ns* shake-up features are seen. There are also structures corresponding to the simultaneous excitation of two valence electrons. The continuous intensity ranging more than 100 eV above the main line is due to shake-off processes in which a second electron is also ionized. The shake-up/shake-off spectra can be used to probe the valence electron structure of a system. What makes this part of the spectrum interesting is that the processes correspond to valence electron excitations between the occupied and unoccupied levels in much the same way as in an optical absorption spectrum. However, since the excitations are caused by the creation of the core hole, the valence states are probed specifically on the core hole site. In Sect. 3.8 shake-up phenomena for adsorbates are discussed in more detail.

Figure 3.4 exhibits the C1s spectrum recorded for $CH_4$ in the gas phase [3.24]. The core ionization gives rise to several discrete features due to the excitation of vibrational motion [3.25]. The peak at lowest binding energy corresponds to the $v = 0$ final state. The peaks at higher binding energies are due to the excitation of one or more vibrational quanta. The splitting between the peaks is about 0.4 eV which is the energy of the vibrational quantum for core

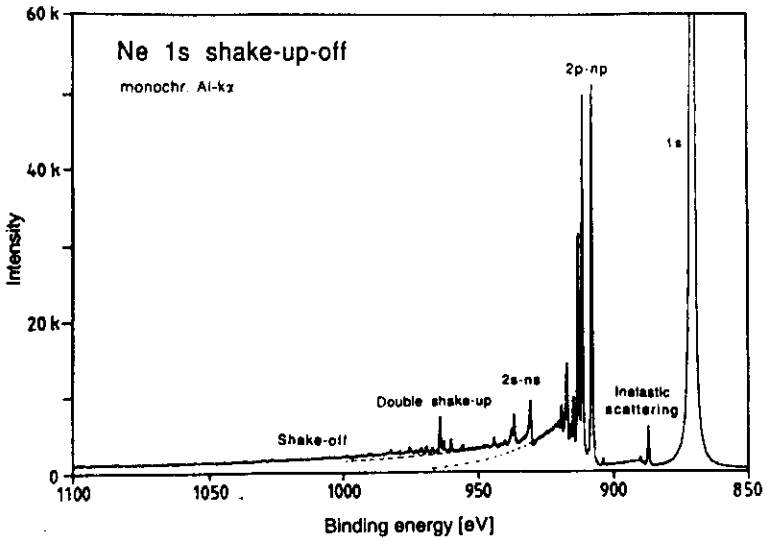


**Fig. 3.3.** The Ne1*s* shake-up spectrum. The shake-up spectrum consists of three groups of lines which correspond to different final state configurations. The lines at 35–55 eV shake-up energy originate from the $1s2s^22p^5np$ final state configurations. The $1s2s2p^6ns$ final state configurations appear at 55–80 eV. At very high shake-up energies, 80–130 eV, three hole two particle configurations (double shake-up lines) can be seen. At 46.7 eV above the main line the first shake-off continuum starts. The peaks denoted inelastic scattering are due to dipole excitations of other Ne atoms for the photoelectrons

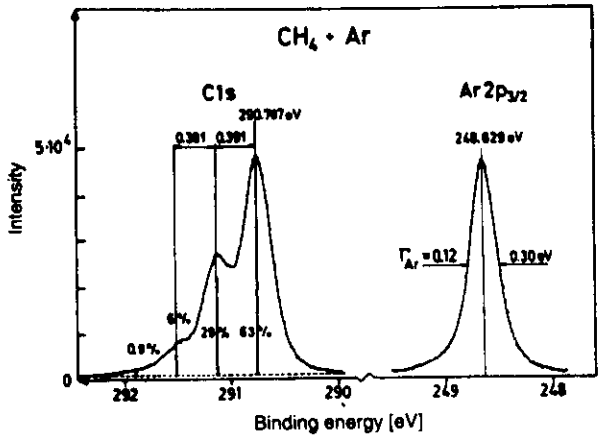


**Fig. 3.4.** Gas phase *C* 1*s* spectrum of methane with resolved vibrational levels. The bars in the figure are obtained by a numerical fit to the spectra



ionized $CH_4$. In an extended system a large number of vibrational modes may be excited and discrete features are no longer seen. Instead, a general broadening of the spectra is obtained. Vibrational excitations most often give the dominating contribution to the photoelectron line widths. This effect may also lead to temperature-dependent broadenings of the spectra [3.26, 27]. The role of vibrational broadening will be further discussed in Sect. 3.7.

## 3.2 Instrumentation

In this section we will briefly describe the instrumentation used for the high-resolution core-electron spectroscopy reviewed in the present chapter. The instruments have been constructed and built at the Department of Physics in Uppsala. The same type of equipment is now commercially available through Scienta Instrument AB in Uppsala.

The photon source generally used for the spectra in the present chapter is a monochromatized Al-$K_\alpha$ source. Some of the measurements have been performed with synchrotron radiation. In principle, there is no difference between a line source and synchrotron radiation for the measurement of core-level photoelectron spectra from adsorbates. In some cases it is important to have sufficiently high photon energy to ensure that one is close to the sudden limit (Sect. 3.8). For C 1s, N 1s, and O 1s excitations the laboratory source still produces core-level spectra of higher quality both regarding resolution and intensity. This is partly due to the fact that longer measuring times can be accepted in the home laboratory. This situation is now changed when the new third-generation synchrotron radiation sources come into operation. In the case of surface core-level shift measurements it is necessary to use tuneable synchrotron radiation in order to obtain the required surface sensitivity.

Figure 3.5 illustrates an outline of the 200 mm radius high-resolution electron energy analyzer [3.28]. The maximum resolution obtained for such an analyzer is 2.7 meV as determined in the gas phase for the Xe *5p* line using a helium lamp [3.28]. There have recently been large improvements in the energy resolution of gas-phase UV photoelectron spectra [3.29]. The analyzer in Fig. 3.5 has successfully been used at the MAX synchrotron radiation laboratory in Lund together with a soft X-ray grating monochromator [3.30]. Due to the high transmission even at high resolutions of the analyzer, spectra of very high quality have been obtained on a bending magnet beamline in spite of the rather low photon flux [3.30].

The high-resolution XPS system used for adsorbate core-level studies is depicted in Fig. 3.6 [3.31]. This is an ultra-high vacuum instrument similar to a gas-phase spectrometer described in detail in [3.32]. The X-ray source consists of a fine-focused high power electron gun, a water-cooled high-speed rotating anode and a wide-angle crystal monochromator mounted on a Rowland circle

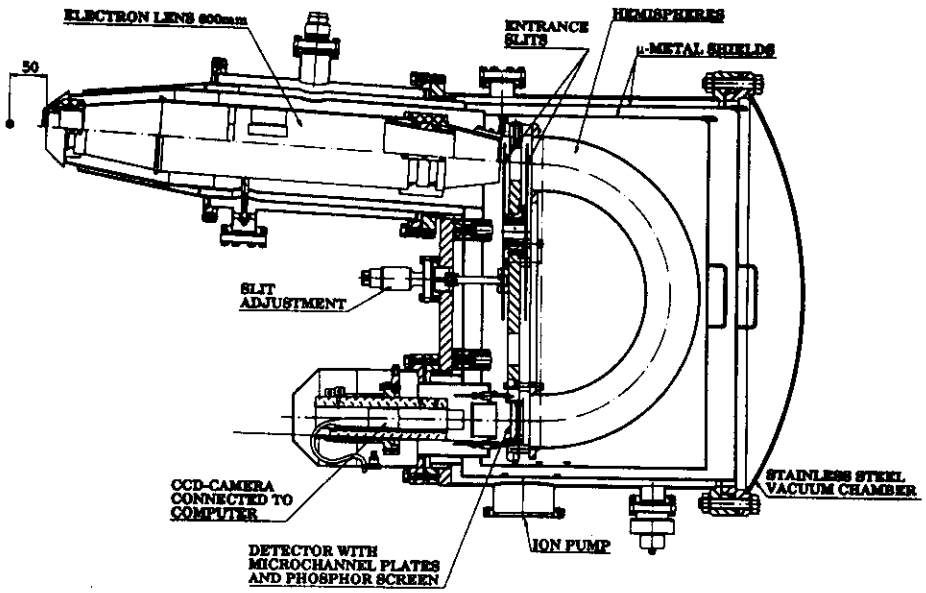


Fig. 3.5. Sectional view of the 200 mm hemispherical electron energy analyzer

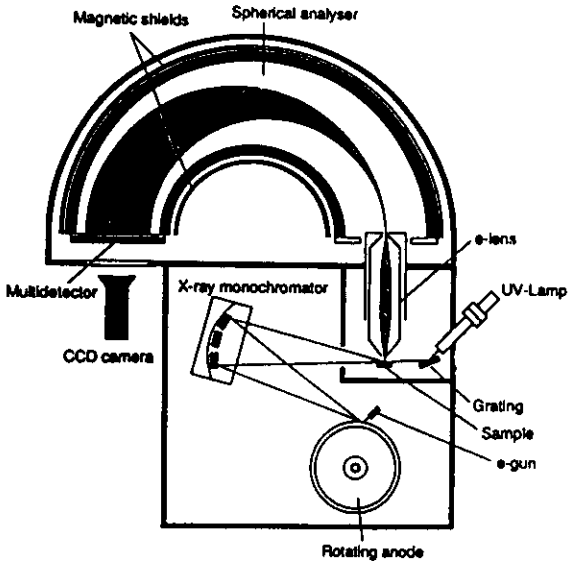


Fig. 3.6. Outline of the high resolution XPS system



(40 cm diameter) arrangement. The electron gun is a two-stage Pierce type gun which provides X-ray powers of 4 kW. The focused electron beam has a diameter of 1.5 mm. The disc of the rotating anode has a diameter of 30 cm and the outer perifery is water-cooled. The water flows in and out through the shaft of the anode. Rotational speeds of 5000 rpm were sufficient for the X-ray powers used. Both the water seal and the vacuum seal are contact-free. This is achieved by a series of narrow cylindrical slits with an engraved multithread system. The slits actively pump themselves and they also allow for efficient two-stage differential pumping. The X-ray monochromator consists of 25 spherically bent quartz single crystals, each of 36 mm diameter. The crystals are mounted in three rows on a large spherical concave surface formed in a large block of optical glass. The monochromator is kept at a constant temperature of 70°C.

The emitted photoelectrons enter through a four-element electrostatic lens into a large hemispherical electrostatic analyzer. These components are enclosed in a double $\mu$-metal magnetic shield. The mean radius of the analyzer is 36 cm. The gap between the spherical electrodes is 15 cm which allows for a large area multidetection system. The detector consists of 2 channel plates in tandem and a phosphorous screen. The light pulses are registered by a CCD (Charge Coupled Device) camera and the readout system is interfaced to a computer.

An overall resolution of at least 0.25 eV can be obtained with the described system. However, the resolution is often reduced to 0.4 – 0.5 eV in order to increase the intensity from the weak adsorbate core levels.

## 3.3 Core-Level Shifts

The existence of chemical shifts is one of the most important aspects of core-level photoelectron spectroscopy. The chemical shifts can be used to distinguish between different chemical species in a sample. In many applications the shift scale is empirically established by studying different reference compounds. Often, however, the shifts have to be interpreted by a comparison to theory. The shifts can also be used to derive information on a more fundamental level about the electronic structure, the structure or the chemical stability of the system. This again requires that the shifts are treated within some theoretical framework.

This section will describe some general aspects of the theory of the chemical shift, especially relating to the question of initial and final states effects. The so-called equivalent core approximation is often useful in order to estimate the properties of the core ionized final state. This approximation will be described in the last part of this section.

### 3.3.1 Initial and Final State Effects

The ionization energy of a system can be expressed as the total energy difference between the ionized ($N-1$ electron) final state system and the initial ($N$

electron) system,

$$E_B = E_{tot}(N-1) - E_{tot}(N). \tag{3.2}$$

For the theoretical evaluation of an ionization energy various approaches can be used to derive the required total energies. When the total energies are calculated using the SCF (Self Consistent Field) method this is referred to as the ΔSCF approach. For the treatment of chemical shifts on this level, separate total energy calculations have to be performed for the initial and final states of the two systems which are to be compared.

There are also other ways to calculate the relevant total energy contributions to the terms in (3.2). Using a Born-Haber type of approach the ionization process is divided into a set of imaginary steps [3.33]. This is done in such a way that some of the energy terms are determined from independent experiments. In this way one can also isolate what type of energy terms are determining the shifts. Such decompositions will be discussed below for the case of adsorbate core levels and for the surface core-level shift in metals.

Using (3.2) we can express the chemical shift between two systems $A$ and $B$ as

$$\begin{aligned}\Delta E_B &= E_{tot,A}(N-1) - E_{tot,A}(N) - (E_{tot,B}(N-1) - E_{tot,B}(N)) \\ &= E_{tot,A}(N-1) - E_{tot,B}(N-1) - (E_{tot,A}(N) - E_{tot,B}(N))\end{aligned} \tag{3.3}$$

The shift is thus determined by two total energy differences: one relating to the initial states and one relating to the final states. Depending on the system the chemical shifts may be dominated by either the initial or final state terms. When one compares the core ionization of two chemically inequivalent atoms in the same system the initial states are the same, and the binding energy shift is entirely due to the difference in total energy of the two final states. The chemical shift between the two chemically inequivalent nitrogen atoms for adsorbed $N_2$ is such a case [3.34, 35]. Similarly when one compares on top- and bridge-bonded CO on Ni(100) one knows that the two adsorption states have very similar total energies [3.36, 37]. In spite of this, large shifts are seen which again have to be attributed to the final-state total energy terms. In other situations, however, the shifts may be mainly determined by the initial-state terms.

Often chemical shifts are treated in a different way which leads to a completely different meaning of the terms initial- and final-state effects. Within the Hartee-Fock approximation the orbital energies have a direct interpretation in terms of ionization energies (Koopmans' theorem). This is obtained under the assumption that all the other orbitals are unaffected by the ionization. However, when a core electron is removed the remaining electrons respond to the suddenly created positive charge. This leads to a contraction towards the nucleus of all orbitals centered at the core-hole site. In a molecular or solid system there is, in addition, a flow of charge towards the core-hole site [3.38, 39]. In fact, in extended systems the ionization often leads to a final state in which the core hole is more or less completely screened by the valence electrons. The lowering of the core ionization energy due to these rearrangements is referred to as the relaxation energy. It is common to define the relaxation energy as the difference between the ionization energy calculated within Koopmans' approximation and the ionization energy calculated on the ΔSCF level. The ΔSCF level, however, is still only an approximation. In a molecular approach the difference between the experimental and the calculated SCF total energies is often referred to as the correlation energy. We will not discuss this term any further. Based on this separation of contributions it is common to separate chemical shifts into two parts, Koopmans' shifts and relaxation shifts (a third shift contribution should be due to differences in the correlation energy). These two parts are commonly referred to as initial- and final-state shifts, respectively. Note that this separation is completely different from the previous separation which was based on initial- and final-state total-energy terms. It is therefore important not to confuse these two approaches. It should also be noted that the initial-state shift defined as a shift on the Koopmans level is a theoretical construction.



There are several reasons why the latter approach has been quite common. Often it is simply assumed that the relaxation energy is the same for the ionization of different atoms in a system or that it is similar for core ionizations in similar systems. The experimental shifts are then compared directly to calculated Koopmans' shifts. This constancy of relaxation energies is quite often the case although it is most difficult to know when it really applies. Another reason for sticking to this type of approach originates from the earlier use of potential models for interpreting chemical shifts, i.e., the notion that the chemical shifts are due to the charge state of the ionized atom. The calculated orbital energies are sensitive to the charge state in much the same way as they are in these potential models. This approach therefore often leads to the interpretation of shifts in terms of atomic charges. The shifts are, in fact, often used as probes of charge states. However, this may lead to most erroneous conclusions. We will not discuss the relationship between these two approaches any further. In the following we will entirely discuss the shifts within a total energy framework.

### 3.3.2 Equivalent Core or $Z+1$ Approximation

One way of getting total energy information relating to the core ionized states is to use the so-called *equivalent core approximation*. The radius of a core orbital is much smaller than that of a valence orbital. The core electrons are therefore located almost entirely inside the valence electrons. The effect on the valence electrons of a core ionization consequently will be nearly the same as if a unit charge were added to the nucleus. Many of the properties of a core ionized atom are therefore the same as the properties of the next element in the periodic table. This is the $Z+1$ or equivalent core approximation. This approximation was used already long ago in the interpretation of optical spectra.

The accuracy of the $Z+1$ approximation depends strongly on which properties of the core ionized system are considered. When calculating metallic

screening energies it has been found that rather large corrections may have to be made [3.33]. All effects which are related to the open core shell are also missing. In those cases when multiplet effects are present, which involve the coupling to the core hole, the $Z + 1$ approximation gives information relating to multiplet averages. Usually when chemical shifts are considered the $Z + 1$ approximation is very accurate. In that case the total energy difference between the same core ionized atom in two different chemical surroundings is considered. In this way the largest errors in the $Z + 1$ approximation cancel out. The only terms which differ are the terms relating to the chemical interaction with the surrounding atoms and especially for this type of terms the $Z + 1$ approximation is quite accurate [3.33]. The validity for the equivalent core approximation for chemical effects is, for instance, well-known for the lanthanides. The properties of lanthanides are very similar over the whole series which means that even the $Z + 14$ approximation is quite accurate. The fact that the approximation is not perfect gives rise to the so-called *lanthanide contraction.*

For many systems information about the $Z + 1$ systems is available which can be used immediately for the interpretation of the shifts. In other cases it is possible to use general chemical know-how for the interpretation of the spectroscopic data. Furthermore, the accuracy of this approximation makes it possible to use the shifts to obtain total energy information on the $Z$ and $Z + 1$ systems.

We will employ this approximation in several parts of the present chapter. We will use it for the interpretation of chemical shifts in Sects. 3.4 and 3.5. In the discussion of vibrational effects in Sect. 3.7 it will be utilized to obtain information about the final-state potential-energy surfaces. The $Z + 1$ approximation is also most helpful for the interpretation of shake-up spectra. The shake-up excitations correspond to electronic excitations in the core-hole state and this approximation can be used to obtain electronic structure information related to this state. In this case, however, one must consider the possibility that the core hole couples to the valence excitations.

## 3.4 Adsorbate Core-Level Shifts

In this section, we will show some examples of how adsorbate core-level shifts can be used to obtain information on the geometrical and electronic structure of small molecules adsorbed on surfaces. The shifts will be discussed in terms of differences in total energies between the initial and final states. In the first part of the section the two main screening mechanisms for adsorbates on metal surfaces are discussed. The remaining part is devoted to selected examples of the application of adsorbate shifts. These examples are the chemical shift between the two nitrogen atoms in $N_2$ which become inequivalent upon chemisorption, the shift between the different adsorption sites for CO, the site selectivity and



molecular orientation sensitivity of the shifts for chemisorbed NO, and the layer dependent shifts for physisorbed $O_2$ on graphite.

### 3.4.1 Final State Effects

When an atom or molecule is adsorbed onto a surface, new final-state relaxation (screening) channels open up which are not present in the free atom or molecule. The surface induced relaxation can lower the final-state energy by several eV. There are two different types of substrate induced screening for an adsorbate: metallic screening and image potential screening.

Metallic screening involves a charge redistribution of the conduction electrons in the metallic system in order to achieve a locally neutral core hole site. The totally screened state can be looked upon as a state in which the screening electron has been taken from infinite distance. Since for a metallic system the appropriate reference level for the binding energy scale is the Fermi energy, we can consider the core ionization process as a core excitation to the Fermi level. The onset in X-ray Absorption Spectroscopy (XAS) corresponds to the creation of a final state where a core electron has been placed in the lowest unoccupied state, i.e. at the Fermi level. This means that the core ionized final state is more or less identical to the state obtained at the X-ray absorption threshold. There is only a negligible difference due to the fact that one electron is actually removed in the photoemission process which is not the case in XAS. This will change the Fermi level by an amount inversely proportional to the total number of valence electrons in the system. Due to this relationship the Fermi level position for the unoccupied valence states as probed by XAS can be derived from the corresponding photoemission binding energy.

Figure 3.7 indicates how the XPS and XAS spectra are related in two different cases of chemisorption. To the right, spectra are shown for a strongly chemisorbed atom, C on Ni(100). The adsorption energy is of the same order of magnitude as the cohesive energy of Ni metal. It is clearly seen how the XPS peak defines the threshold of the XAS spectrum. There is even a change in slope of the leading absorption edge at the peak position of the photoemission line. The same relationship holds also for molecular chemisorption. To the left, the C 1s spectra are shown for CO adsorbed on Ni(100). In this case the intensity is rather low at the X-ray absorption threshold since the main density of states in adsorbed CO is located well above the Fermi level. A similar relationship between XAS and XPS has been obtained in a number of weak chemisorption systems such as CO on Cu, Ag and Au surfaces, showing the existence of metallic screening for the main photoemission line. However, in these systems the main lines may have very low intensities, as discussed in Sect. 3.8.4.

The metallic screening of the adsorbate involves charge transfer from the substrate to the molecule. The degree of charge transfer does not have to correspond absolutely to one electron and the core ionized atom may in many cases be slightly ionic or polarized in the bond to the surface. Information on the electronic structure of the lowest core hole states can be obtained from the $Z + 1$

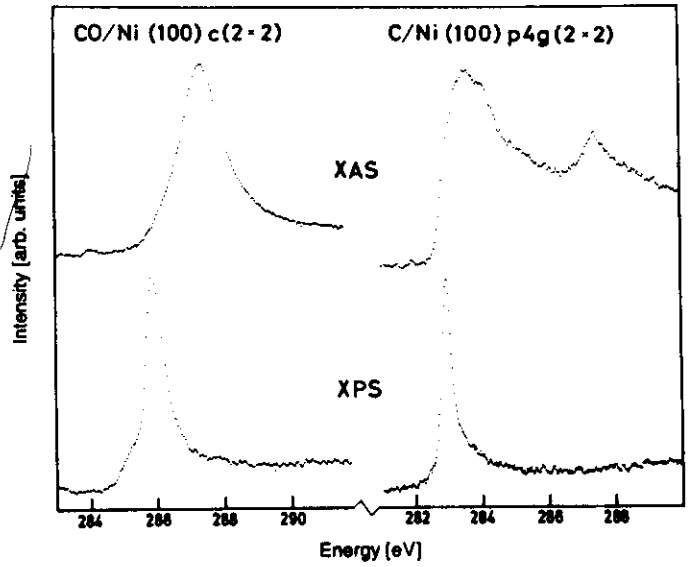


**Fig. 3.7.** C 1s *XA* and *XP* spectra for C/Ni (100)$p_{4g}$ (2 × 2) and CO/Ni (100)c(2 × 2). The XA spectra are shown on a photon energy scale and the XP spectra on a binding energy scale referenced to the Fermi level. Note that the binding energy scale is reversed from the standard procedure

approximation. For adsorbed atomic carbon, the final state is replaced by an adsorbed nitrogen atom. The local electron population does not differ by exactly one unit between carbon and nitrogen since the two atoms have different electronegativities. When ionizing atomically adsorbed C, N and O, the final-state atoms will always have a larger electronegativity than the ground state atoms, leading to a screening by more than one electron. In the case of a chemisorbed rare-gas atom, the final state is similar to an adsorbed alkali atom which is ionic or extremely polarized, and we could anticipate that the charge transfer is much less than one electron.

For an adsorbed molecule such as CO, the metallic screening can be illustrated in terms of changes in the orbitals forming the bonds to the surface. Figure 3.8a shows the projected CO $2\pi^*$ derived density of states for CO adsorbed on Ni(100). In the free CO molecule the $2\pi^*$ orbital is empty, but upon adsorption it becomes slightly populated by the formation of $2\pi$-metal hybrid states. This leads to a splitting into $2\pi^*$ derived states which are bonding and antibonding with respect to the surface (Fig. 3.8a). For CO on Ni the occupied bonding states have mainly Ni 3*d* character whereas the antibonding states have mainly CO $2\pi^*$ character. The core hole will modify the $2\pi^*$ derived states, as shown schematically in Fig. 3.8b for a C 1s hole. The $2\pi^*$ occupancy increases considerably due to the attractive core hole potential. This can be seen in



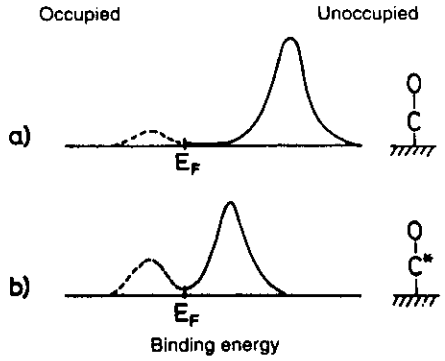


**Fig. 3.8a, b.** A schematic illustration of the CO derived $2\pi^*$ density of states for CO adsorbed on Ni (**a**) in the ground state and (**b**) in the presence of a core hole on the carbon atom

adsorbed NO which is the $Z + 1$ analogue for a C1*s* hole state. In NO, the $2\pi^*$ orbital is occupied by one electron already in the free molecule. The unoccupied $2\pi^*$ derived states are pulled down by 2 eV towards the Fermi level compared to CO. The $2\pi^*$ screening of the core hole in adsorbed CO corresponds to the increased weight of occupied $2\pi^*$ derived states in Fig. 3.8b. This increase can be viewed in two alternative ways; (i) some of the previously unoccupied $2\pi^*$ states are pulled down below the Fermi level due to the core hole potential and become populated, or (ii) the bonding $d$-$\pi$ hybrid orbitals contract towards the adsorbate, thereby increasing their $2\pi^*$ character.

If the interaction between the adsorbate and substrate is weak as for a physisorbed molecule (small orbital overlap), the ionized state cannot be screened by electron transfer from the substrate. The relaxation occurs only by polarization of the substrate, which in the case of a metallic substrate is denoted image potential screening. The ionized atom or molecule is now left in a positively charged state and a charge redistribution in the metal causes a negative polarization charge to build up in the substrate.

Figure 3.9 compares the $1s$-$1\pi_g$ core excitation to the 1*s* core ionization spectrum for $O_2$ on graphite [3.40]. The $1\pi_g$ is a twofold degenerate orbital in the free $O_2$ molecule populated by two electrons. The two electrons have parallel spins giving rise to the paramagnetic state of the molecule. It is immediately seen that the XAS peak appears at lower energy than the photoemission peak. A metallically screened photoemission final state, neutralized by the transfer of an electron from the substrate to the $1\pi_g$ orbital, would have an energy corresponding to the X-ray absorption threshold. Hence, the XPS final state is not the lowest possible core hole state. It is a $1s^{-1}$ ionized state screened by the image potential. Further evidence of the lack of metallic screening in physisorbed $O_2$ is the fact that 1*s* line shows a doublet structure in the 1*s* photo emission spectrum. The molecular paramagnetic splitting of 1.1 eV arising from two final states with different spins ($^4\Sigma$ and $^2\Sigma$) [3.41], is preserved for the adsorbate.

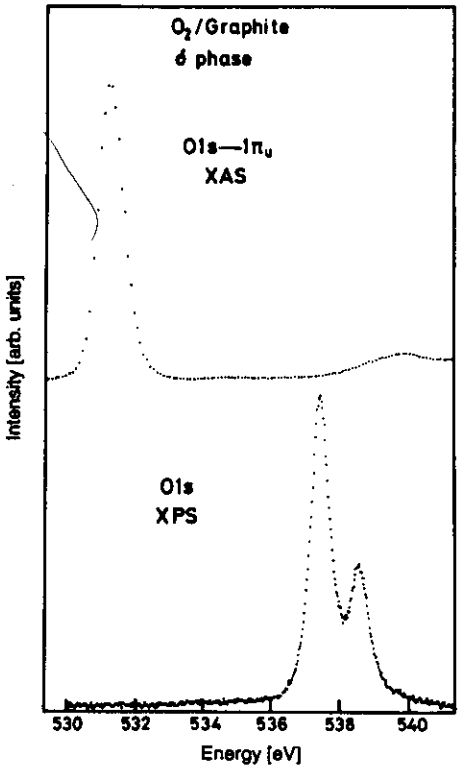


Fig. 3.9. O1s XA and XP spectra for $O_2$ physisorbed on graphite in the $\delta$ phase [3.40]. The XA spectra is shown on a photon energy scale and the XP spectra on a binding energy scale referenced to the substrate Fermi level. Note that the binding energy scale is reversed from the standard procedure. The spectra were recorded at 25 K

### 3.4.2 Chemical Shifts Between Inequivalent Atoms

The XP spectrum of mo'ecular $N_2$ on Ni(100) in the $c(2\times2)$ structure is shown in Fig. 3.10 [3.34]. Due to the perpendicular adsorption geometry, the two nitrogen atoms are inequivalent and two chemically shifted N 1*s* peaks are seen at 399.4 and 400.7 eV binding energies. The component with the lowest binding energy corresponds to the outermost nitrogen atom [3.35]. This identification has been based on different observed angular variations of the photoemission intensities from the two nitrogen atoms due to photoelectron diffraction effects [3.34, 35]. The 1.3 eV shift can be understood in terms of the adsorption energies of the different final state species. Using the $Z+1$ approximation, the N 1*s* ionized final state can be replaced by an adsorbed NO molecule. Core ionization of the outer nitrogen atom leads to adsorbed NO with the nitrogen atom closest to the surface whereas the ionization of the inner nitrogen atom leads to NO with the oxygen end down. The stable configuration of adsorbed NO has the nitrogen atom downwards [3.42, 43]. Ionization of the outer nitrogen atom then



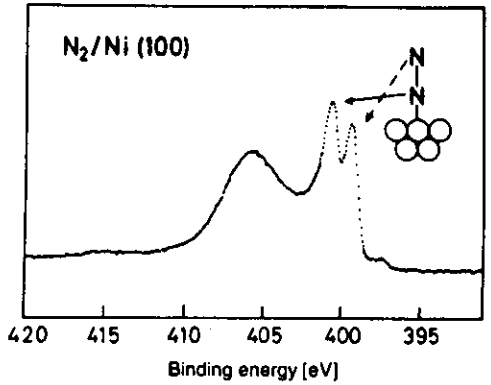


Fig. 3.10. The N 1*s* spectrum for $N_2$ adsorbed on Ni (100) in a $c(2\times2)$ structure. The spectra were recorded at 80 K. The two inequivalent nitrogen atoms are marked in the figure

leads to the most favourable final state, even though the core hole is further away from the surface. This demonstrates that the energetics of the final state screening in a chemisorbed molecule is not directly related to the distance of the core hole to the surface but that it depends on the overall electronic structure of the core-hole state. The difference in adsorption energies between the two NO orientations on Ni is equal to the binding-energy shift of 1.3 eV [3.35].

### 3.4.3 Adsorption Site-Dependent Shift in CO

We will now demonstrate how binding energy shifts can be used to determine the adsorption site of CO on Ni and Pt surfaces. Adsorption of CO on Ni(100) leads to the formation of a $c(2\times2)$ structure at $\theta=0.5$ with all CO molecules in equivalent positions. In this structure the molecules adsorb in on-top sites with the molecular axis perpendicular to the surface and the carbon end downwards [3.44]. For higher CO coverages two new structures appear. This involves the population of other adsorption sites than the on-top sites. At saturation, $\theta=0.67$, a $p(3\sqrt{2}\times\sqrt{2})R45°$ structure appears for which vibrational spectroscopy has proposed that only bridge adsorption sites are populated [3.44]. Between saturation and the $c(2\times2)$ structure a $c(5\sqrt{2}\times\sqrt{2})R45°$ structure develops with a mixture of on top and bridge sites [3.44].

Figure 3.11 shows C 1*s* and O 1*s* spectra of CO adsorbed on Ni(100) in the three different overlayer structures [3.46]. In the $c(2\times2)$ structure the C 1*s* and O 1*s* lines appear at 285.9 eV and 532.2 eV binding energy, respectively. For the $c(5\sqrt{2}\times\sqrt{2})R45°$ structure there are shifts towards lower binding energies and both lines become much broader than for the $c(2\times2)$ structure. Finally, in the $p(3\sqrt{2}\times\sqrt{2})R45°$ structure the line widths become similar to the $c(2\times2)$ spectra with total negative binding energy shifts of 0.5 eV for C1*s* and 0.9 eV for O1*s*. The increased line width for the intermediate structure is thus due to overlapping peaks from the two types of sites which are populated.

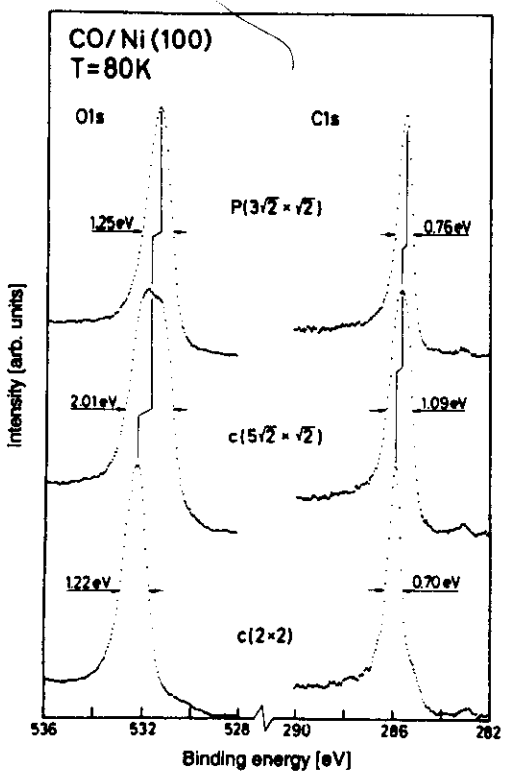


**Fig. 3.11.** C 1*s* and O 1*s* spectra for CO on Ni(100) in the $c(2\times2)$, $c(5\sqrt{2}\times\sqrt{2})R45°$ and $p(3\sqrt{2}\times\sqrt{2})R45°$ structures. The spectra were recorded at 80 K. The half widths of the peaks are indicated in the figure

In the coadsorption system CO + H on Ni(100) a wider range of adsorption sites becomes accessible [3.45]. There are different phases of CO in which the molecules occupy on top, bridge and hollow adsorption sites as seen from vibrational spectroscopy [3.46]. The coadsorbed phases were prepared by first producing a $p(1\times1)$H structure at 80 K and then adsorbing CO at the same temperature with subsequent annealings to different temperatures. At the bottom of Fig. 3.12 the spectra from the clean $c(2\times2)$ overlayer of CO on Ni(100) are shown for comparison. Co-adsorption with hydrogen at 80 K also leads to a $c(2\times2)$ structure with only on top population. The C1*s* and O1*s* peaks shift to higher binding energies by 0.4 eV and 0.7 eV, respectively, relative to the $c(2\times2)$ phase without hydrogen. It is interesting to note that the binding energy positions are similar to the $c(2\times2)$CO phase on Cu(100) which also has on-top adsorption sites. Raising the substrate temperature to 170 K yields a $c(2\sqrt{2}\times\sqrt{2})R45°$ structure. In the spectra two peaks can now be seen with an energy separation of 1.2 eV for C 1*s* and 2.6 eV for O 1*s*. Vibrational spectroscopy shows that also hollow adsorption sites become populated in this phase [3.46]. The relative intensity between the two sites is 1:1. Increasing the temperature to



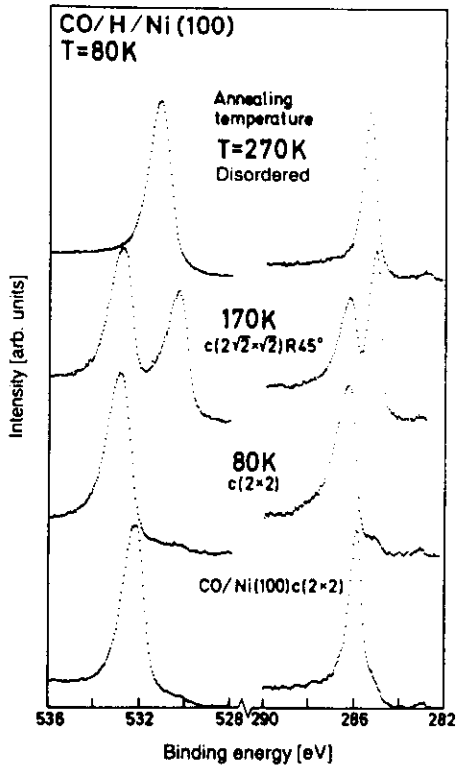


**Fig. 3.12.** XP spectra of the C 1*s* and O 1*s* levels from the CO–H coadsorption system on Ni (100). The spectra were recorded at 80 K after different annealing temperatures. The spectra from $c(2\times2)$-CO on pure Ni (100) are shown for comparison

270 K results in some desorption of CO as well as of $H_2$ ($\Sigma$-desorption), which leaves the remaining CO in bridge sites. The photoelectron spectra in Fig. 3.12 show peaks with intermediate binding energies. The binding energy is very close to the value obtained for the bridge populated $p(3\sqrt{2}\times\sqrt{2})R45°$ structure of the pure CO overlayer.

Similar results are also obtained for Co on Pt(111) [3.47]. Figure 3.13 exhibits the O 1*s* and C 1*s* spectra for three ordered structures of CO; $(4\times4)$, $c(4\times2)$ and $c(5\times\sqrt{3})$ rect [3.48]. The corresponding Pt 4*f* spectra are shown in Fig. 3.20 together with structural models of the overlayer in Fig. 3.21 (Sect. 3.5.2). For the $(4\times4)$ phase, there is only one peak seen in each spectrum at 286.7 and 532.7 eV binding energy, respectively. The binding energies fall in the range typical of on-top sites. The $c(4\times2)$ and $c(5\times\sqrt{3})$ rect structures involve both on-top and bridge sites and a second component is observed at 286.0 and 531.0 eV. The C1*s* binding energy is 0.6 eV larger than for the bridge site on Ni(100) whereas the O1*s* energy is exactly the same. In the $c(4\times2)$ phase ($\theta = 0.5$), equal amounts of sites are populated. For the $c(5\times\sqrt{3})$rect overlayer ($\theta = 0.6$), 2/3 of the molecules occupy on-top sites.

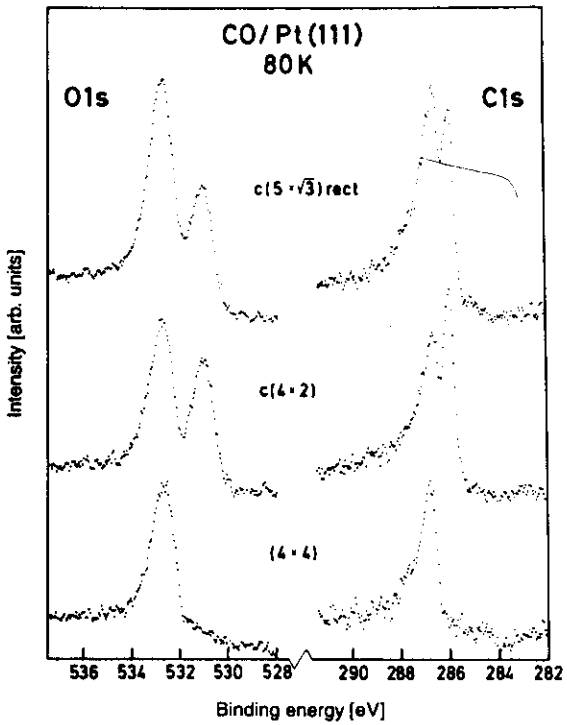


**Fig. 3.13.** C 1*s* and O 1*s* XP spectra from three ordered phases of CO on Pt(111); (4 × 4), *c*(4 × 2) and C($\sqrt{3}$ × 5) rect. The spectra were recorded at 80 K. Backgrounds from clean Pt have been subtracted in both core-level spectra

These examples clearly reveal that there are strong site-dependent binding-energy shifts for adsorbed CO. The shift is about twice as large for O1*s* as for C1*s*. The binding energy decreases with increasing coordination to the substrate atoms, i.e., in the order on-top > bridge > hollow. This is an empirical relationship which could be used in the study of CO adsorption on Ni, Pt and other surfaces. In vibrational spectroscopy a similar empirical rule has been used for many years based on the CO stretch vibration.

The shifts can be understood from total-energy considerations. In the initial state prior to ionization there are only small differences in adsorption energies (a few 100 meV) for the different sites. Hence, the major contribution to the shift must come from changes in the energy of the core ionized state. Within the $Z + 1$ approximation the C 1*s* ionization produces a NO-like final state and the O 1*s* ionization a CF-like final state. The carbon part of the CF molecule contains 'three unpaired' electrons available for bonding, while the 'fluorin' part



of the molecule is completely saturated due to the large difference in electronegativity between the two atoms. For a free carbon atom with four unpaired electrons the adsorption site is such that the coordination to Ni is optimized. On Ni(100) the interaction is so strong that a reconstruction of the Ni lattice occurs with the carbon atoms in the hollow position. Also, CF can be anticipated to maximize the coordination in a similar way. From this it can be concluded that the O 1*s* final-state molecule has its equilibrium adsorption site in the hollow position, which is in agreement with the O 1*s* shift measurements. In order to move the CF molecule to the bridge and on-top sites the spectra show that an energy of 1 and 2 eV, respectively, is required. There is no large difference in electronegativity between the CO and NO molecules. NO is therefore expected to adsorb in a manner similar to CO, only with slightly larger adsorption energies due to the extra unpaired valence electron. Therefore, the variation in the final-state energy is smaller for C 1*s* than for O 1*s*. These chemical arguments have been supported by CI (configuration interaction) calculations of Ni clusters simulating the ionization for on-top and hollow adsorption sites of CO [3.36].

### 3.4.4 Molecular Orientation and Site-Dependent Shifts in NO

The adsorption of NO on Ni(100) is much more complex than the adsorption of CO. No ordered molecular overlayer structures are formed in this system. Figures 3.14 and 15 show how the N 1*s* and O 1*s* spectra develop for different doses of NO at 80 K [3.43]. Already at a dose of 0.3 L, which gives a coverage of 0.04, adsorbate spectra can be observed with a lot of details. At 0.8 L only one peak can be seen in each spectrum indicating a single adsorption site with N 1*s* and O 1*s* binding energies of 398.1 eV and 531.4 eV, respectively. For a dose of 1.2 L a second peak is seen in the N 1*s* spectrum at 1.8 eV higher binding energy. With increasing coverage the second N 1*s* peak increases in intensity and the first one vanishes completely at the saturated surface. In the O 1*s* spectra a second peak is observed at intermediate coverage with 1 eV lower binding energy. At saturation this O 1*s* peak decreases and leaves an asymmetry of the line towards lower energies. It can be noted that there is no clear connection between the double peak structures in the N 1*s* and O 1*s* spectra. The chemical shifts in the two spectra must therefore be of different origin.

The first adsorption state at low coverage has been found to be a lying-down or highly-tilted NO species from studies using X-ray photoelectron diffraction and UPS [3.49]. The second N 1*s* peak is related to a perpendicular NO adsorption state on the surface [3.49, 50]. The large N 1*s* binding energy shift of 1.8 eV between the standing-up and lying-down NO can again be understood using the $Z + 1$ approximation, i.e. by replacing the final-state molecule by an adsorbed $O_2$ molecule. For molecularly adsorbed oxygen only the lying-down geometry has been found on different surfaces [3.51–53]. Therefore the lying-down final state must have the lowest total energy. This is in agreement with our results which give the lowest binding energy for the tilted

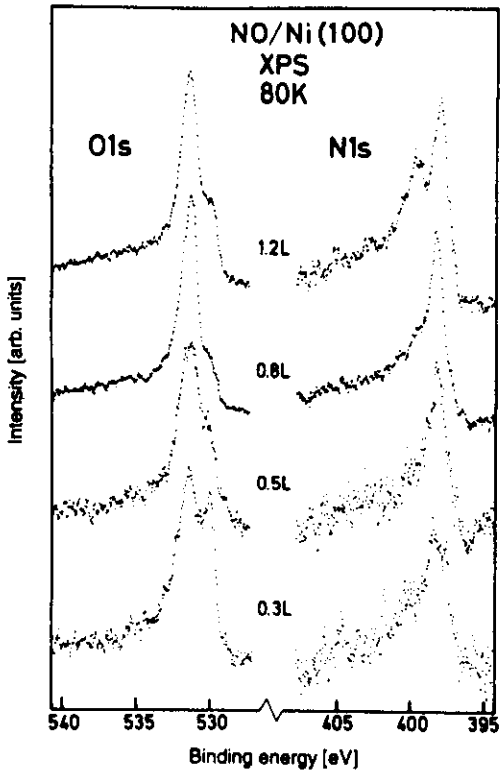


Fig. 3.14. O 1s and N 1s XPS spectra for low coverages of NO adsorbed on Ni(100) at 80 K. The different exposures are indicated in L (1L = $1 \times 10^{-6}$ Torr s)

system. From the N 1s shifts we can estimate that an energy of nearly 2 eV is required to raise molecular oxygen into a perpendicular geometry.

In the O 1s spectra at intermediate coverage the second peak at lower binding energies grows when the perpendicular NO species becomes populated but then nearly vanishes at saturation coverage. From a comparison with vibrational spectra of this system there is an indication that the second peak is related to a hollow adsorption site and the first one to a bridge site [3.45]. For the perpendicular adsorbate the hollow site should then be first populated and with increasing coverage the molecules would be transferred to bridge sites. For perpendicularly adsorbed NO the adsorption site with lowest energy should correspond to the hollow site. This is also found using the $Z + 1$ approximation for the C 1s spectra of CO on Ni(100) where the final state NO-like molecule adsorbs with lowest energy in the hollow site (see Sect. 3.4.3). Applying the $Z + 1$ approximation to the O 1s final state in NO results in a NF-like final-state molecule. The observed shifts indicate that the site dependence of this molecule is similar to that of CF.



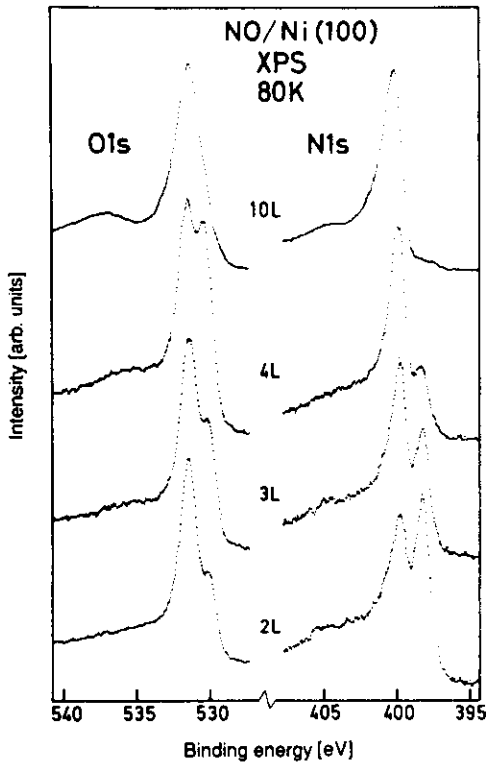


Fig. 3.15. O 1s and N 1s XPS spectra for high coverages of NO adsorbed on Ni(100) at 80 K. The different exposures are indicated in L

For adsorbed NO, core ionization of the different atoms provides complementary information. The N 1s energy is mainly sensitive to the molecular angle relative to the surface whereas the O 1s energy is more sensitive to the local adsorption site.

### 3.4.5 Physisorption-Induced Shifts in $O_2$

Next we will turn to a physisorption system, $O_2$ on graphite, where the ionized molecules are screened by an image potential. The phase diagram of $O_2$ on graphite is rather complex and involves many different phases. However, at 25 K only two MonoLayer (ML) phases are of interest. Starting at low coverage the $\delta$ phase is formed up to a coverage of 0.67. In this phase the molecules bond with the molecular axis nearly parallel to the surface [3.55, 56]. As the coverage is increased the molecules change their orientation. In the $\zeta 2$ phase, which completes the monolayer, the molecules are nearly standing up with a tilt angle of $37 \pm 10°$ from the surface normal [3.55, 56]. The molecules continue to grow

in the perpendicular orientation when multilayers are formed. The angle of the molecular axis to the surface normal decreases with thickness [3.56].

Figure 3.16 depicts the O 1s spectra relative to the Fermi level from submonolayer coverages to roughly 10 ML of $O_2$ on graphite [3.57]. The paramagnetic splitting of the O 1s line was discussed in Sect. 3.4.1. The gas phase spectrum shown at the bottom of the figure has been shifted by 1.4 eV to lower binding energies in order to line up with the monolayer spectrum [3.41]. The lower binding energy for the physisorbate is due to the polarization of the surface (image potential screening) and the neighbouring molecules, as discussed in Sect. 3.4.1. The spectra from the submonolayer phases ($\theta_0 = 0.5$ and the $\delta$-phase) are virtually identical showing similar local surroundings. Due to the change in adsorption geometry, the spectrum changes between the $\delta$- and $\zeta$2-phases. The more 'upright' adsorption geometry of the molecules in the $\zeta$2-phase results in (ideally) two inequivalent oxygen atoms with respect to the surface. The atom closest to the surface will be more efficiently screened by the image potential [3.40]. By the same mechanism the librational motion (frustrated

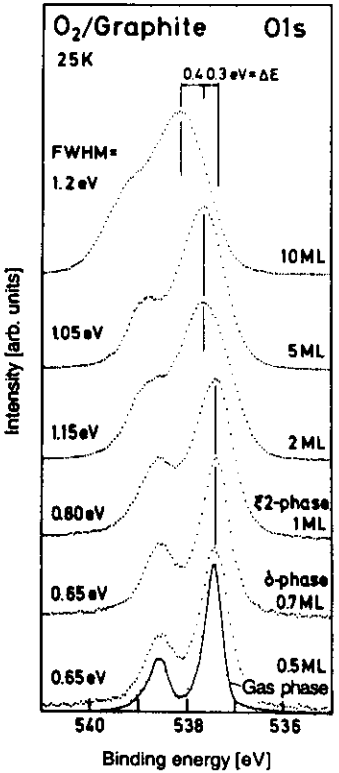


Fig. 3.16. The O 1s spectra for several coverages of $O_2$ physisorbed on graphite are shown. A shifted gas phase spectrum (from [3.41]) is inserted in the lower part of the figure. The number of different MonoLayers (ML) is indicated (right). The FWHM of a gaussian line profile of the quartet component is given (left), as well as the shifts in binding energy between different coverages (upper part)



rotations) of the molecules leads to a continuous range of binding energies whicl further broadens the spectrum [3.40].

At a coverage of 5 ML of $O_2$/graphite, a narrowing of the O 1s peak i observed. This is partly due to the fact that the intensity from the low-energ component (first monolayer) is suppressed by the covering layers. At th coverage corresponding to 10 ML, the growth mode is not known. The smeare out spectral features are due to inhomogenous sample charging, which is cause by the growth of crystalline oxygen. The shift in the second layer is 0.5 e towards higher binding energy relative to the monolayer. This type of shifts ha previously been interpreted in a simple model based on the distance between th ionized atom and the image plane [3.58–62]. However, it turns out that it is als important to consider the polarization screening of the surrounding molecule both in the same layer and between adjacent layers [3.58]. Furthermore, it ha been seen from calculations that the internal molecular screening depends on th external screening [3.63]. This indicates that it is not possible to separate th different screening channels, i.e. the internal screening, the image potentia screening and the response from the surrounding molecule, into independen contributions only based on shift measurements. This requires studies of th satellite features related to the different screening contributions (Sect. 3.8.2).

## 3.5 Surface Core-Level Shifts

In Fig. 3.2 we saw for Yb that the core-level binding energy of a surface atom ca be different from that of a bulk atom. The binding energy difference between th surface and the bulk is denoted Surface Core Level Shift (SCLS), $\Delta E_s$.

$$\Delta E_s = E_B(\text{surface}) - E_B(\text{bulk}). \qquad (3.4$$

Using the SCLS the properties of the surface atoms can be probe [3.33, 64–68]. In this section we will at first briefly review how an expression fo the SCLS can be derived which relates it to surface energies and surfac segregation energies. The $Z$-dependence of the SCLS will then be discussed fo the 5*d* transition elements and it is shown that the theory provides a straightfor ward explanation of the shift curve. Furthermore, the influence of adsorbates o the SCLS will be discussed. The different effects of physisorbed and chemisorbe molecules will be treated. Using spectra for CO/Pt(1 1 1) it will furthermore b demonstrated how the Pt 4*f* spectra can be used to probe what adsorption site are populated.

### 3.5.1 Clean Metals

A most useful description of the surface core-level shift is obtained if one treat the surface and bulk ionization energies in terms of separate Born-Haber cycle

[3.33, 64]. This derivation is based on a total energy description of the initial and final states, as discussed in Sect. 3.3. The metallic screening of the final states is explicitly taken into account [3.33]. The Born-Haber cycles are used to decompose the total energy expressions into terms which can be obtained in independent ways. These terms can be divided into two categories: terms which represent the energies on the atomic level associated with the screening of the core hole site and terms which describe how the properties of the initial and final state atoms are renormalized in the solid state. When chemical shifts are considered, the first type of terms cancel out and we need only consider how the ionized atom bonds to the lattice before and after the ionization in the bulk and at the surface. In the initial state for a bulk ionization this defines a term which is equal to the cohesive energy of the metal. To derive the final-state energy we here use the $Z + 1$ approximation. Note, however, that this approximation is not a necessary ingredient in the theory. The bonding energy of the final-state atom to the lattice can be expressed as the sum of two terms, the cohesive energy of the $Z + 1$ element plus a term representing the solution energy of a $Z + 1$ atom in the host system. Usually the latter term is rather small and we will, for the sake of clarity, neglect it in the present discussion. The core-level binding energy in the bulk of a metal can then be expressed as

$$E_B(\text{bulk}) = A + E_{\text{coh, bulk}}(Z) - E_{\text{coh, bulk}}(Z + 1) \tag{3.5}$$

where $A$ contains all terms in the Born-Haber cycle which do not depend on the detailed environment of the core ionized atom.

For the surface the same type of derivation can be made. The only terms which change, are the terms which describe the bonding, i.e. the cohesive energies. The bonding energy is reduced at the surface due to the reduced number of coordinating atoms. Instead of (3.5) we then obtain the equation

$$E_B(\text{surf}) = A + E_{\text{coh, surf}}(Z) - E_{\text{coh, surf}}(Z + 1) \tag{3.6}$$

with the only difference that the bulk cohesive energies are replaced by surface cohesive energies. The surface cohesive energy can be expressed as $E_{\text{coh, surf}} = \alpha E_{\text{coh, bulk}}$ where $\alpha$ is a constant less than one. The cohesive energy for a surface atom is lower than for a bulk atom due to the reduced number of bonds at the surface. For a close-packed surface a typical value of $\alpha$ is 0.8. The difference between the bulk and surface cohesive energies is referred to as the surface energy $E_{\text{surf}} = E_{\text{coh, bulk}} - E_{\text{coh, surf}}$. The SCLS, $\Delta E_s$, can thus be expressed as

$$\begin{aligned}\Delta E_s &\approx E_{\text{surf}}(Z + 1) - E_{\text{surf}}(Z) \approx (1 - \alpha)\,[E_{\text{coh}}(Z + 1) - E_{\text{coh}}(Z)] \\ &\approx 0.2\,[E_{\text{coh}}(Z + 1) - E_{\text{coh}}(Z)].\end{aligned} \tag{3.7}$$

The value of $\alpha$ above will depend on the packing of the surface. The surface energies are larger for more open surfaces and hence one will also observe larger surface shifts.

Figure 3.17 shows the experimental surface shifts for the close packed surfaces of the 5d transition elements [3.69]. It is seen that there is a sign reversal



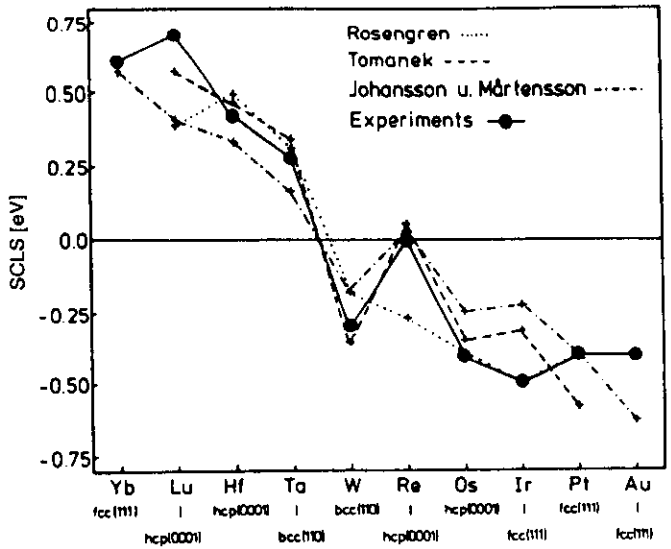


**Fig. 3.17.** Comparison of the experimentally determined SCLS of the 5*d* transition metals with the results of different theoretical approaches. Only the values of the close-packed surfaces are included

of the shift in the middle of the series. For the early elements the shift is positive while at the end of the series the shift is negative. The experiments are compared to three different evaluations of (3.7) [3.33, 70, 71]. As can be seen the theoretical curves reproduce the experimental results quite well. The details of this comparison are discussed in [3.69] where it is also shown that the real reason for the kink between W and Re is the fact that the Z-dependence of the surface energies is different for bcc, fcc and hcp metals.

From (3.7) one can directly see the reason for the general behaviour of the SCLS in Fig. 3.17. The cohesive energy for the 5*d* transition elements is dominated by the *d*-electron contribution. The 5*d* density of states can occupy a total of 10 electrons per atom. The character of the 5*d* states varies over the density of states. The states at the bottom of the band are bonding and the states at the top of the band are antibonding. For the first elements in the series only bonding states are occupied and the cohesive energy increases with atomic number. The cohesive energy has a maximum in the middle of the series and after this the antibonding states begin to be filled which reduces the cohesive energy as the *d*-band is further filled. With this functional form of cohesive energy it is directly seen from (3.7) that the shifts will be positive for the early elements and negative for the late elements.

Another interesting property of the SCLS is that it can be directly related to surface segregation energies. This can be seen from Fig. 3.18. The ionization of a bulk atom creates a final-state impurity in the bulk of the system. In terms of the

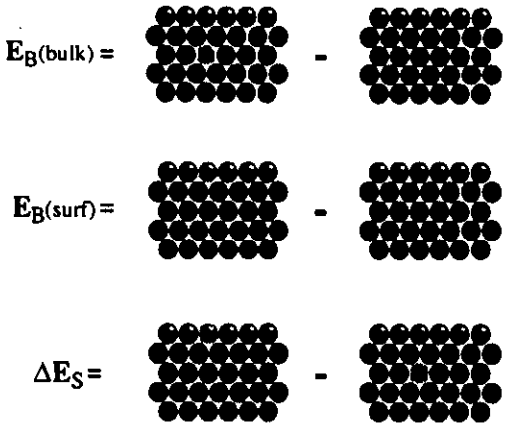


Fig. 3.18. Illustration of the correspondence between the SCLS, $\Delta ES$, and the surface segregation energy of the final state impurity. The final state can to a good approximation be represented by a $Z + 1$ impurity

bonding to the neighbours this atom behaves like a bulk $Z + 1$ impurity. In the corresponding way a core ionized surface atom behaves like a $Z + 1$ impurity at the surface. The two situations are sketched in the figure. It is then immediately seen that the energy difference between the two systems, i.e. the SCLS, corresponds to the surface segregation energy of the $Z + 1$ impurity. In an analogous way the shift between an atom in the bulk of a metal and an atom at a metallic interface, as was observed in Fig. 3.2, has a direct interpretation in terms of interface segregation energies [3.18]. This coupling to thermochemical data is particularly direct and powerful for metallic systems.

### 3.5.2 Adsorbate-Induced Shifts

In the presence of adsorbates the binding energies of the surface atoms change. The magnitude of the shifts is in some way connected to the interaction strength. For weak interaction as in physisorption the influence on the surface atoms will be very small. In the case of strong bonding, however, one can expect substantial shifts for the surface atoms although it is important to realize that a small shift does not exclude strong interaction. This can also be caused by compensating effects in the initial and final states.

Figure 3.19 shows the $4f_{7/2}$ spectrum for an Au(110) surface without any adsorbate and after the adsorption of $N_2$ and CO. The pure-metal spectrum shows a surface shifted component at lower binding energies. The adsorption of $N_2$ has no effect on the surface core-level shift. This indicates that $N_2$ physisorbs on the Au(1 1 0) surface which is consistent with other observations [3.72]. When instead CO is adsorbed the spectrum is seen to change drastically. This is a direct sign of chemisorption [3.73]. The original surface component decreases in intensity. Simultaneously, a new component appears at the high-binding-energy side of the main peak. The adsorption of CO affects the binding energies



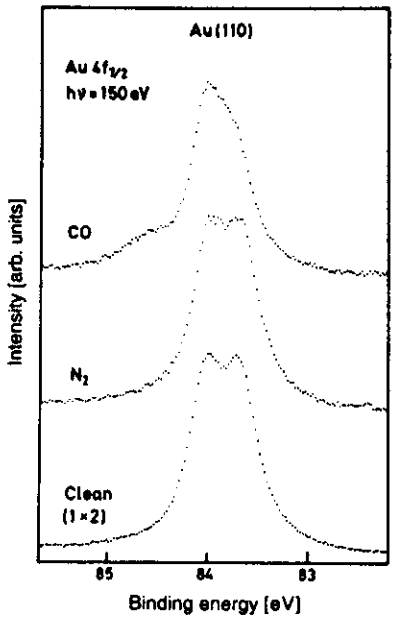


Fig. 3.19. $4f_{7/2}$ photoelectron spectra f Au(110) with and without adsorbates. The go surface exhibits a $2 \times 1$ reconstruction. No o dered CO overlayers could be observed wit LEED

of the surface atoms to the extent that the sign of the SCLS is even reversed. Th fact that the whole surface layer does not shift, again demonstrates the very loca character of the chemical shift.

In the theoretical treatment of SCLS outlined above the presence of a adsorbate enters by adding terms which represent the adsorption energies in th initial and final states, respectively. To a good approximation the adsorptio energies can be associated with the adsorbate and with the atom or atoms t which it is directly coordinated. For on-top adsorption only one surface atom i coordinated to the adsorbate. In this case the SCLS will be modified by th adsorption-energy difference between the molecule adsorbed on the $Z$-meta substrate and the molecule adsorbed in the same geometry on the $Z + 1$-meta substrate. If the adsorbate is more strongly bonded to the $Z$-metal this wil introduce a positive contribution to the shift. This is the expected direction fo CO on Au since CO will bond more strongly to gold than to the $Z + 1$ elemen which is mercury. In fact, in the latter case we expect no chemisorption bond a all.

For other geometries of the adsorbate the treatment becomes more in volved. For bridge adsorption each molecule is coordinated to two substrat atoms. The adsorption energy per coordinated substrate atom (or per bond) i therefore half the adsorption energy. In the final state one substrate atom i

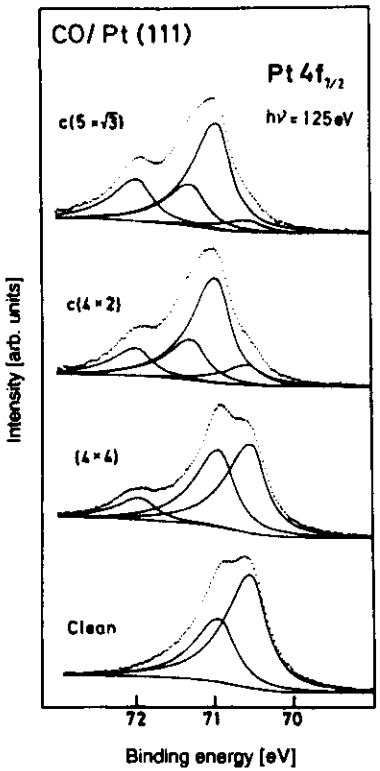


**Fig. 3.20.** $4f_{7/2}$ photoelectron spectra for Pt(111) for the clean metal and for three different CO adsorption phases. The overlayer structures are described in Fig. 3.21. The spectra were recorded at liquid nitrogen temperature

replaced by a $Z + 1$ atom. This defines a term which represents the energy of a bond between the $Z + 1$ atom and the bridge-bonded adsorbate. If we assume that this energy is not sensitive to the fact that the other substrate atom, to which the adsorbate coordinates, is still a $Z$ atom and not a $Z + 1$ atom, then this energy will define an energy which is half the bridge-site adsorption energy on the $Z + 1$ substrate. With these assumptions the modification of the surface shift for bridge adsorption is, thus, half the difference between the bridge-site adsorption energy on the $Z$- and $Z + 1$-metals. If for a certain system the adsorption energies (in the initial and final states) are similar for the on-top and bridge adsorption sites (which is usually the case where both types of sites can be populated) this leads to an expected shift between a free surface atom and a bridge-bonded molecule being about half of the shift to an on-top bonded molecule.

In Sect. 3.4.3. the C 1*s* and O 1*s* spectra for CO on Pt(111) were discussed. These spectra could be used to separate on-top and bridge bonded species. In Fig. 3.20 the Pt $4f_{7/2}$ spectra are shown for the same phases as were discussed



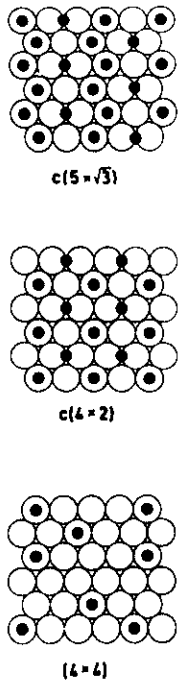


**Fig. 3.21.** Illustration of the investigated CO/Pt(111) adsorption phase The three phases correspond to adsorbate coverages of $\Theta_{CO} = 0.19$ ($4 \times 4$ $\Theta_{CO} = 0.5$ ($c(4 \times 2)$) and $\Theta_{CO} = 0.6$ ($5\sqrt{3} \times \sqrt{3}$) in substrate units. Th fraction of on-top adsorbates for the three phases is 100%, 50% and 67% respectively

above, i.e. the $(4 \times 4)$, $c(4 \times 2)$ and $c(5 \times \sqrt{3})$rect phases [3.74]. The propose structures for these phases are depicted in Fig. 3.21 [3.75]. At the bottom o Fig. 3.20 the spectrum for the clean surface is shown. As can be seen there is surface shift towards lower binding energies in accordance with the discussio above. It can also be noted that the surface sensitivity is such that the surfac peak actually dominates.

In the $(4 \times 4)$ phase the intensity of the original surface peak is reduced. A the same time a new peak appears on the high-binding-energy side of the bul peak. The adsorbate induced shift of this peak relative to the unperturbed pea is 1.41 eV. In the $c(4 \times 2)$ and $c(5 \times \sqrt{3})$rect phases the unperturbed surface pea decreases even further. In these cases there are two new surface components: th one interpreted as linearly coordinated CO and a new peak which has a bindin energy almost half way between the on-top coordinated peak and the un perturbed surface peak (shifted 0.73 eV relative to the pure surface). This ne peak corresponds to the Pt surface atoms which coordinate bridge bonded CO In accordance with the discussion above this leads to an intermediate shif Actually, the shift is reduced by a factor close to two. This might naively b anticipated.

The surface shifts are thus directly related to the local coordination of th adsorbates. It is also interesting to note that the surface peak corresponding t

the uncoordinated Pt surface atoms is unaffected by the adsorption. This demonstrates the extremely local character of the shifts. It is clear from this example and the previous discussion of the shifts in the adsorbate levels that the core-level data provide most detailed information on the geometrical arrangement of the adsorbates. Furthermore, the local character of the probe makes it independent of long-range order of the adsorbate structures.

## 3.6 Core-Level Line Shapes

There are a number of effects which determine the shape of a core-level spectrum. Most often the observed spectrum can be viewed as a convolution of the fundamental spectral shapes due to these individual effects. Some contributions, however, may be interconnected in a more complicated way which makes it necessary to consider the effects in a unified manner. In this section we will assume that the effects are separable. We will briefly discuss the various contributions both in the language used for molecules and in a solid-state language.

The different line-shape contributions are sketched in Fig. 3.22 for a free molecule as well as for a solid [3.9]. These are due to the spectrometer resolution function, the finite life-time of the core-hole, inelastic scattering of the photoelectrons, electronic shake-up and shake-off processes and vibrational excitations.

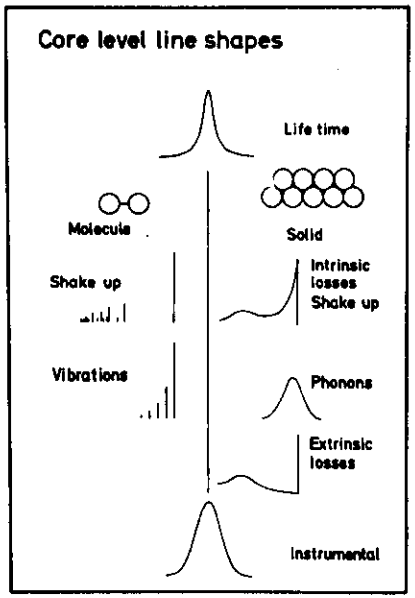


Fig. 3.22. Summary of different line shape contributions for a free molecule and for a solid



Each core level has an intrinsic width due to the finite lifetime of the hole state. The decay is due to radiative and non-radiative processes involving electrons in orbitals outside the core hole (Sect. 3.1). There is usually very little chemical influence on the decay rate and the intrinsic width is essentially an atomic property. The lifetime broadening has a Lorentzian shape. For the C 1s, N 1s and O 1s lines, which are mainly treated in the present contribution, the FWHM (Full Width at Half Maximum) of this contribution is only of the order of 0.1 eV [3.76] and can usually be neglected. For other core levels, however, the Lorentzian broadening may be much larger. There are also rare cases when the intrinsic line shape is more complicated than a simple Lorentzian function. This occurs for instance when the one electron state interacts strongly with other states of similar energy [3.77, 78].

As discussed in the preceding sections, core ionization leads to a modification of the other orbitals in the system. This perturbation gives rise to shake-up and shake-off satellites as shown for the Ne 1s spectrum in Sect. 3.1. Figure 3.22 schematically shows typical shake satellite spectra for a molecule and for a solid. In the molecule the shake-up part of the spectrum consists of a number of discrete transitions due to excitations from occupied to unoccupied orbitals like in Ne. In solids the electronic states form continuous bands. In metals there are filled states up to the Fermi level and empty states right above the Fermi level. The ionization will thus create excitations with energies all the way down to zero. This shake-up contribution gives rise to characteristic core-line asymmetries [3.79]. Other shake-up satellites are due to the creation of collective plasmon excitations or interband transitions and are seen as discrete features in the spectra. It could be noted that for metals the distinction between shake-up and shake-off becomes less meaningful because of the continuous character of the transitions for electrons excited to states below the vacuum level. The shake-up satellites are discussed in detail in Sect. 3.8.

For a molecule or a solid the removal of a core electron usually leads to the excitation of vibrational motion. This is due to the fact that the potential energy curves for the atomic motion are different before and after ionization. The effects of these processes for the spectral shape are indicated in Fig. 3.22 for a molecule and for a solid. In a molecule only a limited number of modes can be excited and the final vibrational excitations can be described in terms of discrete states. In the solid the atomic motion is instead treated in terms of phonons. The band character of the phonons creates a continuous broadening function, which is often considered to be of Gaussian shape. Note, however, that the phonon excitations may generate an asymmetric broadening as well. An identification of the different broadening mechanisms simply on the basis of the type of line profile (Lorentzian, Gaussian or asymmetric) may be dangerous. The vibrational broadening effects are further discussed in Sect. 3.7.

In solids there are satellites due to energy loss events experienced by the escaping photoelectron. These are denoted extrinsic losses. It is often difficult to distinguish between intrinsic (shake-up/shake-off) and extrinsic satellites since they may have very similar energies. Such a separation may, in fact, be rather superficial since it is based on the assumption that the photoemission process

can be treated as a sequence of well separated events. In Fig. 3.22 a typical extrinsic loss spectrum is shown. For a more detailed discussion of extrinsic loss processes see [3.80].

For adsorbates the energy loss contribution can, in general, be neglected. The photo-ionization takes place in the outermost layer of the sample and the photoelectrons are emitted directly into the vacuum. The detection of inelastic loss satellites would require that electrons which are emitted into the solid or along the surface undergo large angle scattering processes. However, both the elastic and inelastic scattering are strongly peaked in the forward direction for typical XPS kinetic energies (Chap. 4). The probability that an electron from the adsorbate layer reaches the spectrometer after only one inelastic scattering event is therefore low (unless the detected electrons are emitted at grazing angles). This makes it reasonable to interpret the complete satellite spectrum in terms of shake-up processes.

The final contribution which is illustrated in Fig. 3.22 is the instrumental-resolution function which in many cases is the limiting factor for what broadenings can be detected. The resolution may vary considerably but is typically of the order of 0.4–1 eV in core-level photoelectron spectra, although a resolution down to about 0.1 eV can be achieved under certain conditions. The main broadening is usually due to the exciting radiation. Using monochromatized Al-$K_\alpha$ a width of the order of 0.2 eV can be obtained. Similar or smaller widths can also be achieved using synchrotron radiation, especially for shallow core levels which require relatively low photon energies. The situation for synchrotron radiation will, however, further improve also for higher photon energies in the near future with the new third-generation synchrotron-radiation sources [3.81].

In a photoelectron spectrum from a condensed system there is always a background corresponding to the ionization of other core and valence levels and Auger transitions (this contribution is not included in Fig. 3.22). The background is due to photoelectrons and Auger electrons which have undergone several inelastic loss processes during their way through the material. The exciting X-rays penetrate rather deep into the material and the individual loss processes usually involve relatively low energies. This means that the electrons which contribute to the energy-loss tails may originate from large depths and the total inelastic intensity in a spectrum is therefore quite significant. This may cause difficulties when investigating weak satellite spectra from adsorbate layers.

## 3.7 Vibrational Effects

For adsorbates the core-level line widths are often dominated by vibrational effects. In this section we will discuss how these effects can be described and quantitatively understood. After a general introduction the widths of the adsorbate 1*s* lines will be discussed for C, N and O on Ni(100). For these systems



the vibrational broadenings can be modelled by employing the $Z + 1$ approximation and using data from surface structure and surface phonon measurements. The temperature dependence of these lines is also described. After this, the line profiles for adsorbed CO are discussed. In this case it is important to consider the intramolecular motion as well as the motion of the adsorbate relative to the surface. Finally, the importance of vibrational broadening for metal spectra is discussed in connection with the observation of temperature-dependent Yb 4*f* line widths.

### 3.7.1 The Franck-Condon Principle

If the core ionization leads to changes of the interatomic distances and/or the force constants, then vibrational motion is excited in the final state. The ionization is usually treated within the Born-Oppenheimer approximation, which implies that the nuclear motion can be decoupled from the electronic motion. This allows the total wave function to be factored into one nuclear and one electronic part which are solutions to separate equations. Figure 3.23 depicts the potential-energy curves for the nuclear motion for two different cases. The lower curve in each figure corresponds to the initial state and the upper curve to the final state of a particular electronic transition, such as a core ionization. The vibrational states are characterized by quantum numbers $v$ and $v'$ for the initial and final states, respectively. In Fig. 3.23 it is assumed that only

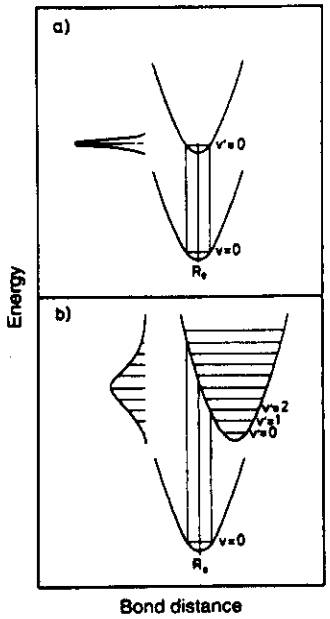


**Fig. 3.23a, b.** Initial and final state potential energy curves describing a photoionization in two different cases: (**a**) corresponds to a small and (**b**) to a large geometry change due to the ionization, giving rise to small and large line widths, respectively

the $v = 0$ vibrational state is populated. For the transition probabilities to the various vibrational states the Franck-Condon principle is generally applicable. The principle states that the relative transition probabilities for the same electronic transition are given by the square of the overlap between the initial and final-state nuclear-motion wave functions. The situation in Fig. 3.23a refers to a situation where the initial and final state potential energy curves are very similar. The two sets of wave functions are thus approximately the same. In this case only the $v = 0$ to $v' = 0$ overlap is non-zero. In Fig. 3.23b the potential energy curves are quite different and the $v = 0$ wave function is nonorthogonal to a whole series of final-state wave functions with $v' = 0, 1, 2$ etc. This leads to the excitation of a number of different vibrational final states. The C 1*s* ionization for $CH_4$, (Fig. 3.4), corresponds to the latter situation. The C 1*s* ionization leads to a shortening of the CH bond by 0.05 Å [3.25].

In the case of a valence photoionization, Fig. 3.23a corresponds to the ionization of a non-bonding orbital while the situation in Fig. 3.23b pertains to the ionization of a bonding or antibonding molecular orbital. When these arguments were transferred to the case of core ionization one was at first led to the conclusion that the situation in Fig. 3.23a applies. With common definitions of bonding and non-bonding orbitals, which are based on the overlap of the atomic orbitals involved, any core orbital is clearly non-bonding. However, this type of argument was later found to be misleading. The situation in Fig. 3.23b may well occur also for a core ionization. The removal of a core electron leads to substantial modifications of the electronic structure as discussed in Sect. 3.4, which may influence the equilibrium bond distances and interatomic force constants.

### 3.7.2 Vibrational Broadening in Adsorbates

When atoms and molecules are adsorbed on surfaces the vibrational modes which are present in the free molecule remain also in the adsorbate, usually with only slightly modified parameters. Furthermore, due to bonding to the substrate, new vibrational modes will appear. These are related to the translational and rotational degrees of freedom of the adsorbate. These additional modes may lead to large differences between the line profiles of free and adsorbed molecules [3.9].

Another consequence of the vibrational effects is that the line widths may depend on temperature. This is easily seen from Fig. 3.23. A higher temperature leads to thermal population of excited vibrational states. If the initial- and final-state potential energy curves are very similar (Fig. 3.23a) the excited vibrational states will ionize to the corresponding final states ($v = v_i \rightarrow v' = v_i$ transitions). The energies of these transitions are essentially the same as for the $v = 0 \rightarrow v' = 0$ transition and there is no additional broadening of the core-electron line. However, if the potential-energy curves are different (Fig. 3.23b) a higher temperature will lead to larger broadening.



The $c(2 \times 2)$ overlayers of C, N and O on Ni(100) are in many respects similar. They all occupy fourfold hollow sites and they form strong bonds to the substrate. They are interesting in connection with the discussion of vibrational effects since independent information on the initial-state as well as the final-state potential energy curves can be obtained. For the final states the $Z + 1$ approximation can be employed. In this way the C 1*s*, N 1*s* and O 1*s* final states behave very much like adsorbed nitrogen, oxygen and fluorine atoms, respectively. In particular, this implies that the potential-energy curves for the final states can be represented by the curves for the $Z + 1$ elements.

Figure 3.24 compares the 1*s* spectra for C, N and O recorded at 150 K [3.27]. The width FWHM is 0.67 eV for the C 1*s* line, 0.94 eV for the N 1*s* line and 1.42 eV for the O 1*s* line. Figure 3.25 shows the spectra for the $p(2 \times 2)$ and $c(2 \times 2)$ phases of oxygen for two different temperatures (150 K and 600 K). The O 1*s* peak is significantly broader for the $c(2 \times 2)$ phase (1.42 eV compared to 1.18 eV for the $p(2 \times 2)$ phase as measured at 150 K). Furthermore, the O 1*s* line width increases with temperature. Also, for nitrogen there is a temperature effect whereas the C 1*s* line width is essentially independent of temperature.

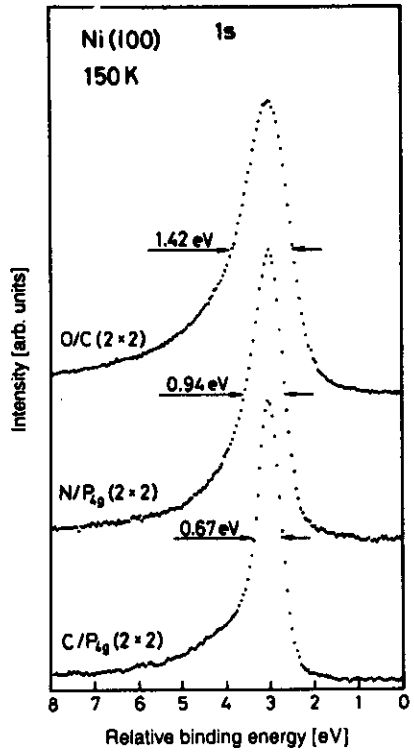


**Fig. 3.24.** C 1*s*, N 1*s* and O 1*s* core line profiles for the atomic $c(2 \times 2)$ adsorbate layers measured at 150 K. The adsorption of carbon and nitrogen leads to a *p4g* reconstruction of the Ni surface layer

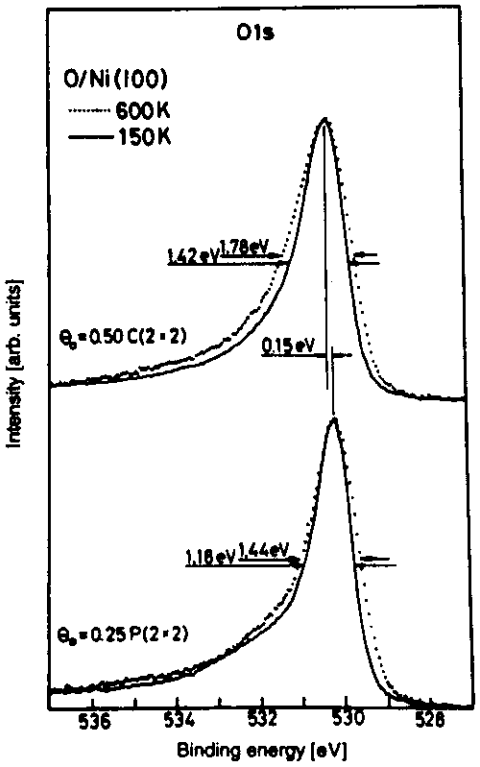


**Fig. 3.25.** O 1*s* core line profiles for the $c(2\times2)$ and $p(2\times2)$ phases of O/Ni(100) recorded at 150 K and 600 K

As seen from the $Z+1$ approximation and the fact that the whole series of atomic adsorbates occupy fourfold sites, the equilibrium geometry does not change parallel to the surface upon core ionization. Hence, for the parallel motion the situation in Fig. 3.23a applies and these modes will not contribute significantly to the broadening. The potential energy curves for the perpendicular motion of C, N and O in $c(2\times2)$ overlayers, as derived in [3.27], are displayed in Fig. 3.26. The curves were obtained within the harmonic approximation using bond distances from LEED and SEXAFS determinations [3.82–84] and force constants from electron-energy-loss data [3.85–87]. If the $Z+1$ approximation is used the curves in Fig. 3.26 are sufficient to estimate the C 1*s* and N 1*s* widths. The C and N potential energy curves are very similar which immediately explains the small C 1*s* broadening. For the N 1*s* ionization, however, there is a substantially larger shift in equilibrium bond distance between the initial and final (oxygen-like) states which leads to calculated vibrational broadenings of 0.55 and 0.84 eV for the N 1*s* line at 150 K and 600 K, respectively. Adding the other broadening contributions yields values in reasonable agreement with experiment [3.27].



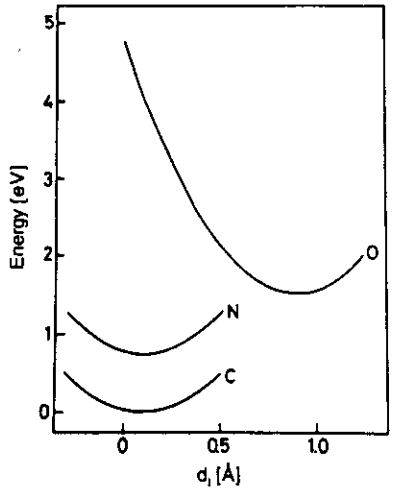


**Fig. 3.26.** Potential energy curves for the vertical motion of C, N and O in the $c(2\times2)$ adsorbate phases derived within the harmonic approximation (see text)

For the O 1*s* ionization, detailed knowledge of the (fluorine-like) final state is lacking. However, it was shown that the observed widths can be reproduced in a consistent way with the same type of model [3.27]. The calculations suggest that the larger widths and the more pronounced temperature effects for the $c(2\times2)$ phase are connected to a shallower potential energy minimum for this phase.

Next we will turn to the line widths of adsorbed CO. Chemisorption of CO leads to substantial broadenings of the core level spectra and it has been demonstrated that these broadenings are almost entirely due to vibrational effects [3.26, 36, 88]. Figure 3.27 depicts the O 1*s* and C 1*s* spectra for the CO/Ni(100) $c(2\times2)$ structure recorded at 80, 230, 300 and 340 K [3.26]. At 340 K the O 1*s* peak has a FWHM of 1.47 eV. The peak has a pronounced asymmetry towards lower binding energies with a relatively distinct cut-off of the low energy tail. As the temperature is lowered the peak becomes narrower (FWHM = 1.22 eV at 80 K) and more symmetric and it shifts slightly to larger binding energy. The full width at the base of the line, however, remains the same. Similar, but smaller effects are seen also in the C 1*s* spectrum. At 340 K the FWHM for the C 1*s* peak is 0.96 eV. Also in the C 1*s* spectrum a temperature variation is seen with a peak width of 0.71 eV at 80 K.

In order to see what effects determine these widths we first consider the free molecule. In the photoelectron spectrum of CO in the gas phase, which has been recorded under similar experimental conditions, widths of 0.71 eV and 0.56 eV are found in the C 1*s* and O 1*s* spectra, respectively [3.89]. The C 1*s* broadening is due to a shortening of the equilibrium bond length upon core ionization. The effect of an O 1*s* hole is instead to lengthen the bond. A difference in the case of the ionization for adsorbed CO is that the core hole is screened by charge

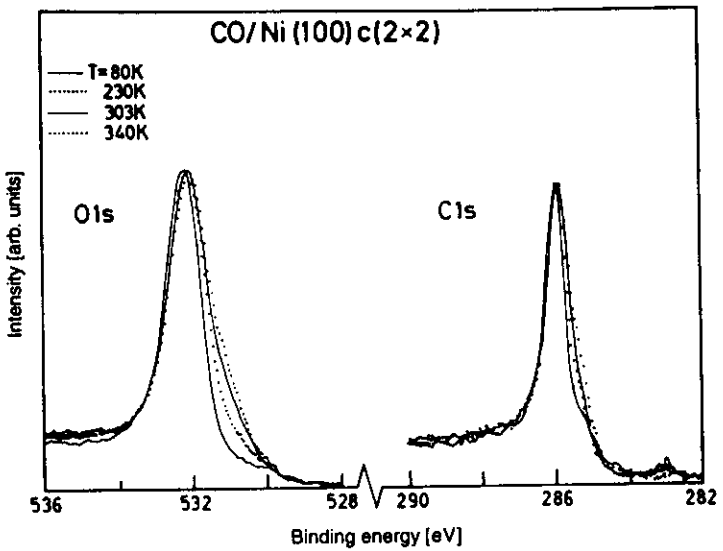


Fig. 3.27. O 1s and C 1s core line profiles for Co/Ni(100) $c(2 \times 2)$ recorded at four different temperatures. Both core lines become broader with increasing temperature

transfer from the substrate. To a first approximation the core ionized adsorbate is therefore similar to a core excited neutral CO molecule. The widths of the C 1s-2p and O 1s-2p transitions have been measured by electron-energy-loss spectroscopy for the free molecule [3.90] and optical absorption (Chap. 6). For the C 1s-2p excitation there is no vibrational broadening at all. This is due to the fact that the population of the antibonding 2p orbital leads to a bond lengthening which compensates the shortening introduced by the core hole. In the case of the O 1s-2p excitation the bond lengthening instead becomes even more pronounced, resulting in a width of 1.3 eV. Already, here, we see an explanation for the larger widths of the O 1s lines. This conclusion is supported by a comparison to the spectra for $Cr(CO)_6$. The metal-CO bond in this molecule is in many respects similar to the bond for an on top bonded adsorbate and the observed C 1s and O 1s widths are 0.82 eV and 1.23 eV, respectively [3.91]. Compared to the core-valence excitation spectra for CO it is seen that there is an additional broadening in the C 1s spectrum which we interpret as due to geometry changes in the Cr–C bond upon core ionization. The O 1s excitation is still dominated by the large bond length increase in the C–O bond.

When CO adsorbs on the Ni(100) surface, new vibrational modes appear which are related to the translational and rotational degrees of freedom of the free molecule. There are, in all, six vibrational modes for a diatomic adsorbate. One vibrational mode $\nu_1$ is related to the free molecule C–O stretch. There are three frustrated translation modes: one mode $\nu_2$ is connected to the translation



normal to the surface (Ni–C stretching mode) and two modes are connected to translations parallel to the surface. The remaining two modes correspond to frustrated rotations. The last modes appear as degenerate pairs denoted $\nu_4$ and $\nu_3$, respectively, in the $c(2 \times 2)$ structure.

The $\nu_1$ and $\nu_2$ vibrational energies have been determined to be 256.5 meV and 59.5 meV, respectively [3.92]. The $\nu_4$ mode has been studied by inelastic helium atom scattering, giving a vibrational energy spacing of 3.5 meV [3.93]. From cluster calculations [3.94] and He atom scattering data for CO on Pt(111) [3.95] it can be concluded that the $\nu_3$ mode has a higher energy.

Both the $\nu_3$ and $\nu_4$ modes could give large contributions to hot bands. It has been argued that the frustrated translation modes are of primary importance in the present case. A vibrational energy spacing of 3.5 meV corresponds to a very shallow potential energy surface. This is consistent with the fact that the mobility of CO is large even at 80 K and the general observation that the difference in total energy for different adsorption sites is small [3.96].

In Fig. 3.28 we have schematically drawn initial and final state potential energy curves which qualitatively explain the O 1s spectra. These are shown along lines passing through the top and bridge sites and along the top and hollow sites, respectively. The periodic functions correspond to independent CO molecules at the surface. For the motion of an individual CO-molecule in a more close-packed adsorbate layer one would also have to include the interaction with the neighbouring CO molecules. These differences are, however, not important for the present qualitative discussion.

The ground-state potential energy surface is drawn with a minimum in the top site, an intermediate energy in the bridge site and the highest energy in the

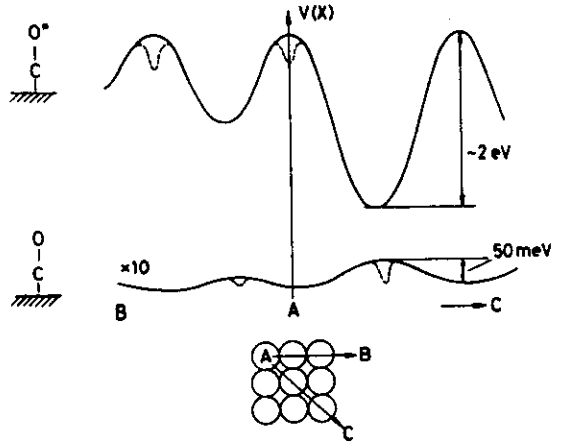


Fig. 3.28. Tentative initial (lower) and O 1s hole state (upper) potential energy curves for CO on Ni(100) along the [10] (arrow A to B) and [11] (arrow A to C) directions

hollow site. This potential-energy surface will lead to a temperature-dependent probability function for the location of the CO molecules at the Ni surface. At low temperatures the molecules will be confined to the region around the top sites. For increasing temperatures there will be an increasing population at larger distances from the top positions, i.e., around the bridge sites and at other intermediate energy sites. In a semi-classical model the spectral line shapes are generated by projecting this distribution onto the final-state potential energy surface [3.88]. The main spectral weight (i.e., the peak position at 532.2 eV) corresponds to transitions from the most probable locations for the CO molecules, i.e. around the top site. The tail towards lower binding energies shows that there is a range of lower final-state energies that can be reached. There are accessible final states with energies as low as 530 eV. The lower intensity of this part of the spectrum is due to the lower population of the corresponding sites in the initial state. From the existence of this low-energy tail it can be concluded that the equilibrium adsorption site (the adsorption site with the lowest energy) for the final state is not the top site. To explain the spectral shape and its

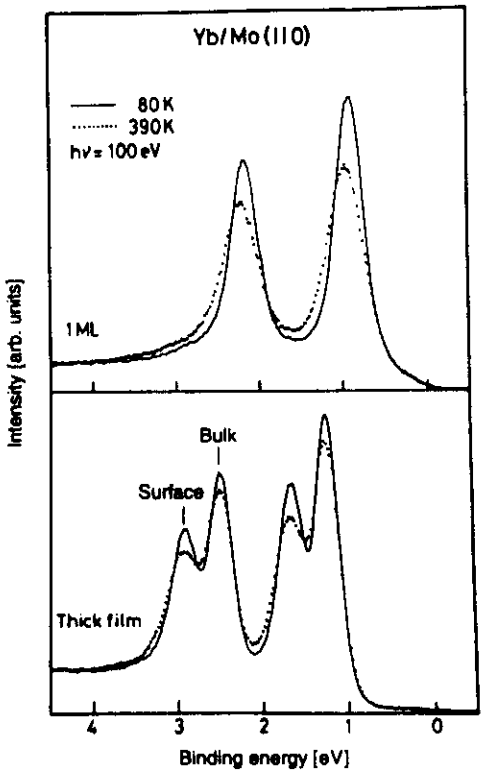


**Fig. 3.29.** Temperature dependence of the Yb 4*f* photoelectron spectra obtained from one monolayer of Yb on Mo(110) and from a thick epitaxial Yb film. The depositions were made at room temperature. The full-drawn spectra were recorded at 80 K and the dotted ones at 390 K. A photon energy of 100 eV was used



temperature dependence it was proposed that the O 1*s* ionized state has its lowest final-state energy in the hollow position, the highest energy in the top site and an intermediate energy in the bridge site and that there is a considerable difference in adsorption energies between these sites. This assumption is totally confirmed by the chemical-shift measurements reviewed in Sect. 3.4.

In Fig. 3.27 it is seen that the C 1*s* line is much narrower than the O 1*s* line. This difference can be explained directly within the present model. What is required is that the final-state potential energy curve is much shallower for the C 1*s* final state. As was seen in Sect. 3.4 this is indeed the case. From the discussion in that section it is also clear that in this case one may anticipate a larger influence from frustrated rotational motion. The $Z + 1$ analogue of C 1*s* ionized CO is NO and, as was discussed in Sect. 3.4, this molecule may, in some cases, adsorb in a tilted fashion. In that case the ionization represents the situation in Fig. 3.23b for the rotational coordinate and that rotational modes may give a larger contribution. To conclude the discussion on CO/Ni(100) we see that a completely consistent description of line shifts and line shapes is obtained.

Temperature effects are also seen in metal spectra. Figure 3.29 exhibits spectra recorded at 80 K and 390 K for 1 ML of Yb on Mo(110) and for a thick Yb film [3.17]. In the monolayer it can be seen that the line width increases with increasir g temperature from 0.42 to 0.57 eV. For the thick film the surface peak shows a similar increase in width from 0.36 eV at 80 K to 0.46 eV at 390 K while the bulk peak only reveals a small change from 0.32 eV to 0.36 eV. The larger width of the surface peak as well as the more pronounced temperature dependence indicates that there are larger vibrational amplitudes at the surface. This can be understood as being due to the increased possibility for movements perpendicular to the surface.

## 3.8 Shake-up Satellites

In this section we will describe the dynamic response of a system caused by the emission of a core electron. Due to this effect each core line is associated with a rich shake-up spectrum, as shown in the Ne 1*s* spectrum in Fig. 3.3. The satellites observed in atoms and molecules undergo large changes upon adsorption on surfaces. The intensity and spectral shape of the satellite features depend strongly on the interaction energy and the local character of the adsorption bond. It will be shown that the energy distribution of these shake-up satellites is determined to a large extent by the local electronic structure of the adsorbate-substrate complex in the presence of the core hole. The shake-up intensities can be used to probe certain properties of the ground state system.

After a general discussion of the shake-up process, a number of examples will be given for different types of adsorption ranging from physisorption to strong chemisorption for atomic as well as molecular adsorbates. We will

describe how the image-potential screening and the polarization of the surrounding adsorbate atoms are manifested in the core-level spectra from weakly adsorbed Ar atoms. For strongly chemisorbed atoms, excitations related to the chemisorption bond can be identified. For oxygen on Ni, a localization of the valence states on the core ionized atom leads to satellite shapes which are dominated by the exchange splitting between the core and valence shells. The spectra from adsorbed molecules such as CO and $N_2$ give rise to intense shake-up satellites. In the case of CO adsorbed on Ag, the so-called *main line* is only a weak feature compared to the giant satellite lines. The satellites in molecular adsorbates on various substrates often have the character of excitations between bonding and antibonding states related to the chemisorption bond.

### 3.8.1 General Aspects

The creation of shake-up satellites is due to the fact that the removal of a photoelectron is much faster than the time required for the rearrangement of the valence electron charge distribution. For the theoretical treatment of the photoionization process the Hamiltonian of the system is considered to change abruptly upon ionization whereas the charge distribution due to the remaining electrons is continuous as a function of time. As a consequence the wave function of the remaining electrons does not correspond to an eigenstate of the final-state Hamiltonian. It has to be expressed as a linear combination of eigenstates of the new Hamiltonian. These eigenstates are observed as separate structures in the spectrum [3.97, 98].

The assumption of an infinitely short time for the removal of the photoelectron is referred to as the sudden approximation. The time for the photoemission event depends on the velocity of the escaping photoelectron and the sudden limit therefore corresponds to high excitation energies. Closer to the core ionization threshold the adiabatic limit is instead approached with, for instance, reduced satellite intensities. The sudden approximation is, in general, quite appropriate in the case of XPS and is the basis for most theoretical treatments of the photoionization process [3.99–101]. It is, however, difficult to formulate strict criteria for the applicability of the sudden approximation, and the energy range within which it is valid is still, to a certain extent, an open question.

Some important sum rules can be derived within the sudden approximation [3.99–101]. As mentioned above, one cannot observe directly the energy of removing an electron from the system while letting all the other electrons in the system remain in their original states. This hypothetical state would be observed if the final-state orbital wave functions were the same as in the initial state. This ionization energy is generally called the *Koopmans energy*. The deviation from this situation depends on how much the orbitals relax as a function of the removal of the core electron. However, it can be shown that the Koopmans energy corresponds to the center of gravity of the complete spectrum including



the shake-up satellites. In general, the main line corresponds to the energetically lowest accessible eigenstate of the core ionized system. If the relaxation energy is large for the lowest state, the sum rule implies that there is considerable intensity for the higher excited shake-up and shake-off states.

Shake-up in atoms and molecules is usually described in terms of orbital excitations in the core-hole system. Only shake-up states which have the same total symmetry as the main core-hole state can appear in the spectra. In general, there are a few transitions which dominate the spectra. Usually it is found that the strongest shake-up transitions involve monopole excitations of the valence electrons, i.e., excitations from occupied orbitals ($nl$) to higher orbitals with the same angular momentum ($n'l$) quantum number.

In solids it is common to distinguish between a few types of shake-up processes depending on the character of the excitations. In metals the core-electron lines are always asymmetric (Fig. 3.22). This is due to shake-up excitations of low-energy electron-hole pairs. Since the density of states is finite at the Fermi level, the excitations have energies ranging all the way from zero. This type of process generates an asymmetric tailing of the core-electron lines towards the high-binding-energy side. Several theoretical treatments of the resulting line shapes have been performed. The most common parametrization which is due to *Doniach* and *Sunjic* [3.79] is based on an analysis of the asymptotic behaviour for long response times of an electron gas to the creation of the core-hole. This type of line shape is often found to describe the experimental peaks quite well and is often used when numerically fitting experimental spectra. There may, however, be other mechanisms as well (Sect. 3.7) which produce asymmetric broadenings which are then artificially taken care of by this model line profile.

Other shake-up excitations are due to plasmons and interband transitions. The energies of these transitions are often rather insensitive to the presence of the core hole and therefore coincide with the energies of the inelastic loss processes. For this reason it may often be difficult to distinguish between intrinsic (shake-up) and extrinsic loss processes for solids. Some of the interband transitions, however, may have a more localized character and are thereby to a larger extent influenced by the core hole. In Ni, for instance, there are shake-up satellites which correspond to different local $3d$ configurations in the presence of the core hole.

A major difference between core ionization of a free and an adsorbed molecule is connected to the additional screening in the latter case (Sect. 3.4.1). The charge redistribution connected with the screening from the substrate leads to additional shake-up features connected to the new screening channels. There are two different types of shake-up excitations that become important for an adsorbate. First, there are local excitations confined to the adsorbate-substrate complex. In this case it is important to explicitly take the effect of the core hole into account. Second, there are excitations in the substrate due to the long-range screening of the adsorbate.

### 3.8.2 Substrate Excitations for Adsorbed Argon

The image charge screening for weakly bonded adsorbates was described in Sect. 3.4.1. The ionization of an adsorbed rare-gas atom will be screened in this way. There are cases when the bonding of rare-gas atoms to the substrate could involve some chemical contribution. However, even if this is the case the charge transfer part of the screening will only involve very small charges and the image potential screening will dominate, as discussed in Sect. 3.4.1.

Figure 3.30 compares Ar 2*p* spectra recorded for the free atom [3.22] and three different situations of Ar adsorbed or graphite: a multilayer (14 ML) of Ar, 1 ML adsorbed on two spacer layers of Xe, and 1 ML adsorbed directly on the

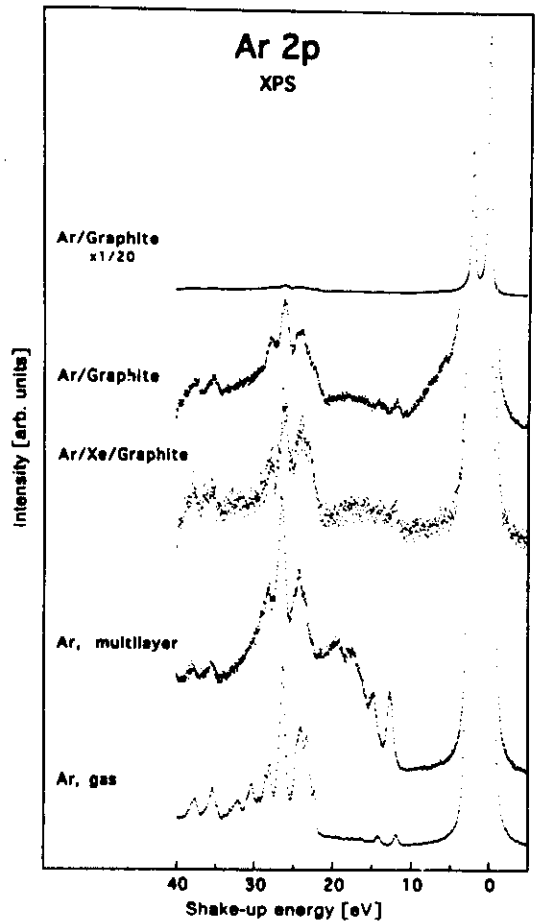


**Fig. 3.30.** XP spectra showing the Ar 2*p* shake-up region for Ar in the gas phase, 14 monolayers on graphite, 1 monolayer adsorbed on two layers of Xe condensed on graphite and 1 monolayer adsorbed on graphite. The spectra have been aligned to the position of the Ar $2p_{3/2}$ peak and normalized to the intensity of the 2*p* main peaks. The energy scale is relative to the $2p_{3/2}$ ionization energy



graphite surface [3.102]. The gas-phase shake-up spectrum is strongly dominated by monopole transitions [3.22]. The shake-up energy region 20–35 eV is due to excitations of 3*p* electrons into Rydberg levels, i.e. 3*p*-*np* transitions. At higher shake-up energies, satellites due to 3*s*-*ns* transitions appear. These excitations are caused by the relaxation of the atomic orbitals upon the creation of the core hole. The weak features appearing in the region 12–20 eV are attributed to inelastic scattering of the outgoing electrons through 3*p*-*ns* dipole excitations.

In the multilayer situation, the atomic shake-up features at 20–40 eV are still present. The main lines maintain their Lorentzian shapes and there is a large band gap in the spectrum. The most pronounced difference compared to the gas-phase spectrum is that the inelastic scattering contribution above 12 eV has increased considerably. This is to be expected for a condensed Ar film where the outgoing electrons have to pass through many Ar layers. The Ar/Xe/graphite spectrum has a number of similarities with the multilayer spectrum. The main lines are Lorentzian-shaped. There is a large band-gap in the spectrum and the atomic shake-up features in the region 20–40 eV are essentially identical for the two situations. Note, also, that there is still some intensity in the energy region corresponding to the atomic dipole excitations.

The spectrum obtained when a monolayer of Ar is adsorbed directly on graphite resembles that of the Ar/Xe/graphite system. The atomic monopole shake-ups are identical and appear at the same shake-up energy as in the Ar/Xe/graphite spectrum. The atomic excitations in the energy region 12–20 eV are also present for Ar/graphite. However, it is immediately seen that extra intensity has emerged on the high-binding-energy side of the main lines, which is not present in the previous situations.

For a physisorbed system, there are two screening contributions which have to be considered, in addition to the atomic relaxation: screening via the formation of an image charge in the surface and screening due to the polarization of the surrounding atoms in the adsorbate layer (Sect. 3.4.5). If these excitations contribute to the screening of the core hole they have to be connected to characteristic excitations in the substrate as well as in the surrounding Ar atoms. The first process explains the shake-up intensity close to the main lines, whereas the latter one gives rise to the atomic excitations observed in the region 12–20 eV.

For a number of reasons it was concluded that the atomic dipole excitations are not dominated by inelastic processes. They are part of the shake-up spectrum [3.102]. For instance, the spectral features disappear at low coverages where Ar adsorbs in a disordered phase with well separated atoms indicating that these excitations are due to the polarization of the surrounding Ar atoms.

The shake-up processes involving substrate excitations can be identified by comparing with inelastic scattering data. For graphite, the electron-energy-loss spectrum reveals a distinct loss at 6 eV, which is interpreted as due to a plasmon exciton [3.103]. If the ionization of an Ar 2*p* electron is accompanied by this plasmon excitation, a 6 eV satellite is expected for each of the two spin-orbit split main lines, i.e., at shake-up energies of about 6 and 8 eV relative to the

$2p_{3/2}$ ionization energy. This is in agreement with the spectrum in Fig. 3.30. This satellite is therefore interpreted as due to the image charge screening.

It is now interesting to compare the image potential screening induced shake-up excitations for Ar adsorbed on other substrates. Figure 3.31 displays the spectra for 1 ML of Ar adsorbed on graphite, Ni(100) and Ag(110). The shake-up peaks related to the atomic relaxation are still present, but they are considerably broadened for adsorption on Ni and Ag. Such broad shake-up peaks are generally associated with chemisorbed species, as will be explained in Sect. 3.8.3. Ar on Ag(110) has recently been found to behave spectroscopically like a chemisorbed system [3.104]. The broadening is thus explained by a hybridization between the unoccupied atomic Ar levels and the unoccupied bands of the metal substrate. The same conclusion can be made for Ar/Ni(100).

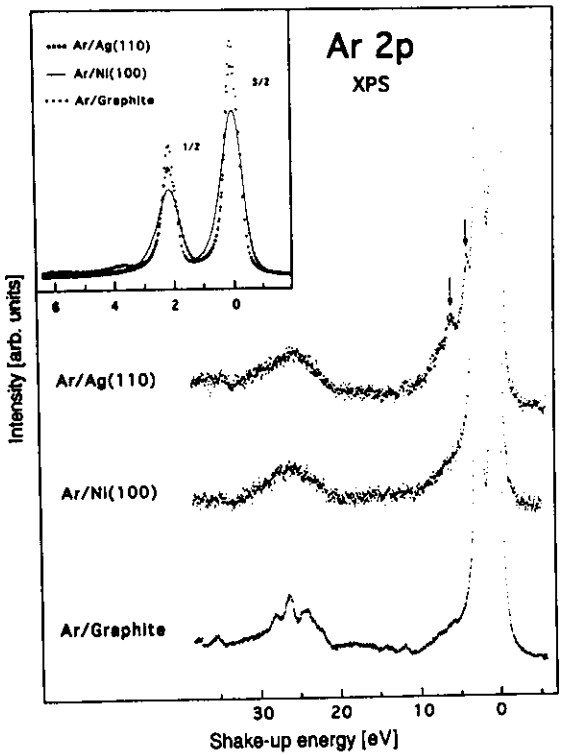


**Fig. 3.31.** XP spectra for adsorbed Ar monolayers on graphite, Ni(100) and Ag(110) showing the Ar 2*p* shake-up region. The main lines are inserted in the top of the figure. The areas of the peaks have been normalized to each other. The energy scales are relative to the $2p_{3/2}$ ionization energy



If we now turn to the low-energy shake-up energy region, two sharp peaks in the Ar/Ag-spectrum are observed at 3.7 and 5.8 eV, respectively. In the Ag 3*d* XP spectrum, sharp satellites appear at 3.8 eV below the main peaks corresponding to unresolved bulk (3.87 eV) and surface (3.63 eV) plasmon losses [3.105–107]. The two peaks in the Ar 2*p* spectrum are interpreted as due to Ag plasmon excitations accompanying the ionization of the two Ar 2*p* components. Since the polarization charge is set up at the surface, it is most likely that the shake-up process is determined by excitations of Ag surface plasmons.

A comparison between the Ar 2*p* main peaks for the three systems is shown in the inset of Fig. 3.31. The 2*p* peaks are much broader in the case of Ar/Ni, whereas the widths of the 2*p* peaks for Ar/Ag are similar to those of Ar/graphite. The broadening effect for Ar/Ni is explained in terms of substrate excitations which have a much larger contribution at low energies than for Ar/Ag [108]. In addition to these low-energy excitations, there are substrate excitations stretching down to about 10 eV for this system, as seen in Fig. 3.31.

The features due to substrate excitations and the excitation of surrounding Ar atoms have a total intensity of $7 \pm 4\%$. The part due to atomic relaxation amounts to $10 \pm 5\%$, which can be compared to the value for the free atom ($13 \pm 5\%$). It may be added that the decrease of the atomic contribution is significant and is an effect of the presence of the substrate. The shake-up intensities are related to the degree of modification of the valence orbitals upon ionization. Therefore, it seems that the presence of an image screening charge in the substrate leads to a smaller contraction of the orbitals for the adsorbate than for the free atom.

### 3.8.3 Local Excitations in Strongly Chemisorbed Atoms

For chemisorbed atoms the possibility of metallic screening will give rise to new shake-up processes connected to the charge transfer from the substrate to the core ionized adsorbate. This extra screening channel will change the valence electronic structure of the adsorbate significantly when the core hole is created. From the series of atomic adsorbates, C, N and O on Ni(100), we will demonstrate that the dominating shake-up processes in these types of systems are mainly localized to the adsorbate-substrate complex.

Figure. 3.32 shows the satellite spectra from the $c(2 \times 2)$ overlayers of C, N and O on Ni(100) [3.109]. Both the energy and intensity of the satellite peaks increase from C to N to O. The main shake-up peaks in the C1*s* and N1*s* spectra appear at 7.0 eV and 10 eV above the main lines, respectively. In the O 1*s* spectrum the satellite is split into at least three states with shake-up energies 10.6 eV, 13.2 eV and 20 eV with maximum intensity for the 13.2 eV state.

The atomic adsorbates form hybrid states between the 2*p* and metal 4*sp* states [3.110, 111]. The occupied 2*p*–4*sp* bonding states appear in the region 4–6 eV below the Fermi level and have mainly adsorbate 2*p* character. There is also some hybridization between 2*p* and metal 3*d* states giving rise to states which are located closer to the Fermi level [3.111]. It has been shown by XAS on

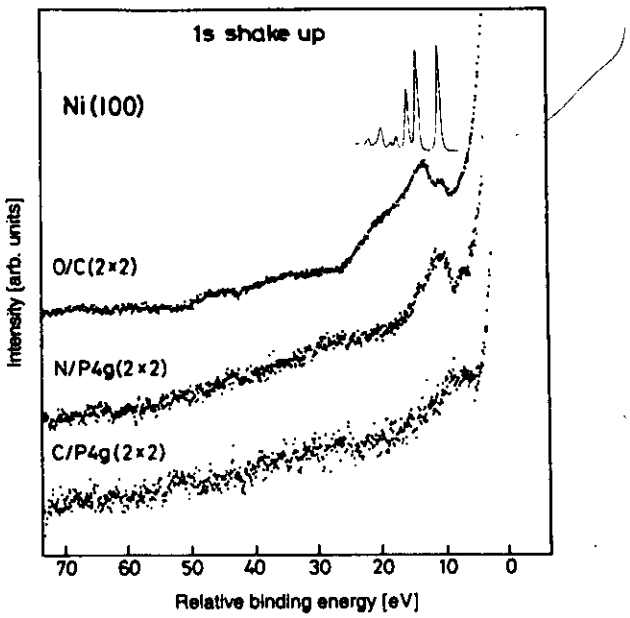


**Fig. 3.32.** 1*s* shake-up spectra of C, N and O adsorbed on Ni(100). The backgrounds from the clean surface have been subtracted. The spectra are aligned according to the main lines. The 2*p*-*np* region of the Ne 1*s* shake-up spectrum from [3.21] has been inserted for comparison with the oxygen shake-up spectrum. The Ne spectrum is shifted by 27 eV to allow the first shake-up peaks in the spectra to coincide

atomic adsorbates, that there exist states with 3*p* character on the adsorbate in the region 3–5 eV above the Fermi level [3.110]. The satellite peaks in Fig. 3.32 are related to shake-up excitations from the bonding 2*p*–4*sp* hybrid states to 3*p* states [3.109]. For the free atom this corresponds to monopole excitations. The energies of these transitions can be estimated using the $Z + 1$ approximation. The shake-up excitations in the C 1*s*, N 1*s* and O 1*s* spectra are then viewed as valence electron excitations in adsorbed nitrogen, oxygen and fluorine, respectively. The valence excitation energy increases with atomic number for the present adsorbates which is also seen from a comparison with optical data for the free atoms [3.112].

In the O 1*s* spectrum there is some fine structure which is not seen in the spectra from the other adsorbates. The final state in the O 1*s* ionization is a fluorine-like species. The adsorption of fluorine on metals has a strong ionic character, leading to an $F^-$ ion with a closed 2*p* shell [3.113]. This implies that the O 1*s* final state of the adsorbate is essentially isoelectronic to a free Ne atom. This makes it interesting to make a comparison with the shake-up spectrum of Ne (Fig. 3.3). A shifted part of the 2*p*–*np* shake-up region in Ne [3.21] is inserted



in Fig. 3.32 above the O 1*s* spectrum. A striking similarity between the two spectra may be noted. The interpretations of the individual peaks in the shake-up spectra are similar. The first two peaks at 10.6 and 13.2 eV in the oxygen spectrum are assigned to 2*p*–3*p* excitations split into upper and lower states by exchange interaction with the 1*s* core hole. The shoulder of the 13.2 eV peak and the broad structure at around 20 eV are interpreted as excitations into higher members of the *np* lower and upper Rydberg series. There are also some tendencies of fine structure in the shake-off continuum related to 2*s*–*ns* excitations and double shake-up processes in Ne (see Fig. 3.3).

The 1*s*–2*p* exchange splitting in the O1*s* satellite spectrum is a direct signature of a localization tendency of the 2*p* shell. This may be compared with the well-known satellite in the Ni 2*p* spectrum where a similar localization of the 3*d* shell in presence of the core hole leads to multiplet splitting of the local 2*p*–3*d* configuration [3.114].

There are parts of the O 1*s* spectrum which are more directly related to the interaction with the substrate. In Fig. 3.33, the O 1*s* spectra from oxygen on Cu(100) and Ni(100) are compared [3.110]. There are clear differences both in line widths and line profiles between the two oxygen core levels. The peak from O/Ni is substantially broader than the O/Cu peak and also more asymmetric. For O/Cu, the line is almost symmetric. In this case a weak but distinct shake-up

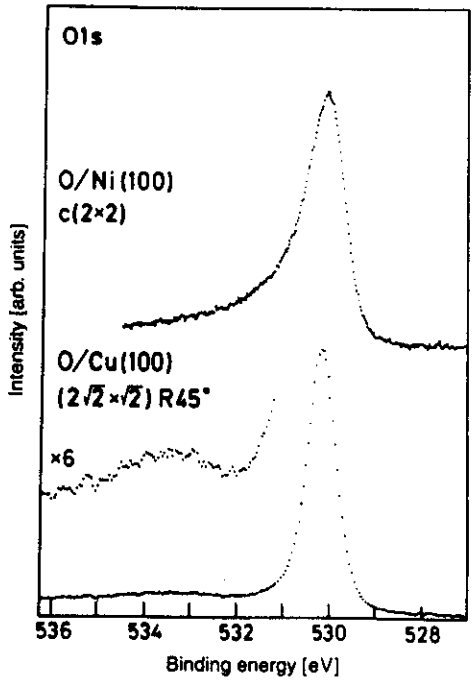


**Fig. 3.33.** XP spectra of the O 1*s* level in the $c(2\times2)$ and $p(2\sqrt{2}\times\sqrt{2})R45°$ phases from O on Ni(100) and Cu(100), respectively. The spectra were recorded at 80 K

structure may be observed about 3 eV from the main line. The $2p$–$3d$ hybrid states can explain these differences [3.110]. In Ni, these states are located in the vicinity of the Fermi level. This enables low energy shake-up excitations which give rise to the asymmetric line profile. For Cu these states are nearly filled and located 2 eV below the Fermi level resulting in a discrete shake-up feature.

### 3.8.4 Chemisorption-Induced Excitations in Adsorbed CO and $N_2$

The adsorption of CO and $N_2$ leads to spectacular shake-up spectra with intensities which are much higher than for the main lines. The interpretation of these giant satellites has been much discussed for more than 15 years [3.31, 34, 115–125]. The various models were recently reviewed [3.126]. Only the interpretation proposed by the present authors will be given below.

Figure 3.34 shows the C 1$s$ and O 1$s$ shake-up spectra for the CO/Ni(100) $c(2\times2)$ structure and for $Cr(CO)_6$ measured in the gas phase [3.31, 91]. The comparison with carbonyls is interesting since the local bonding between adsorbed CO and the substrate is similar to the bonding in the carbonyls. The features in the carbonyl spectra are sharper and the shake-up peaks are better resolved. However, there is a striking similarity between the positions of the main features for adsorbed CO and for the carbonyl. The same characteristic differences between the C 1$s$ and O 1$s$ spectra are seen for both systems. The

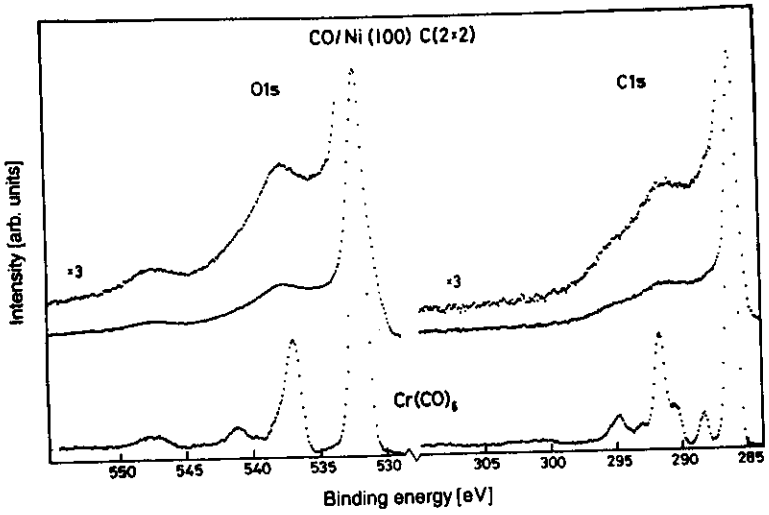


Fig. 3.34. XP spectrum of the C 1$s$ and O 1$s$ regions for CO/Ni(100) $c(2\times2)$ and $Cr(CO)_6$ in the gas phase. The clean Ni background spectrum has been subtracted. The energy scale of the $Cr(CO)_6$ spectra has been shifted by 7.3 eV (C1$s$) and 7.5 eV (O1$s$) in order to allow the main lines to coincide. The spectra were recorded at room temperature



similarity between the two sets of spectra demonstrates that the shake-up energies are dominated by the local electronic structure of the metal-CO system.

The C 1$s$ and O 1$s$ shake-up spectra are significantly different. Three shake-up structures are observed in both spectra, although the shake-up features appear at quite different energies. The difference between the C1$s$ and O1$s$ shake-up spectra demonstrates the necessity of taking the effects of the core hole explicitly into account when treating the shake-up transitions.

Before discussing the interpretation of the shake-up spectra, we will make a comparison with spectra from $N_2$ on Ni(100) [3.34]. The $N_2$ molecule is isoelectronic with CO and the spectra show some similarities in the gas phase. The adsorption of $N_2$ in a perpendicular geometry leads to two inequivalent nitrogen atoms, as discussed in Sect. 3.4.2. The shake-up spectra from the two different atoms have been separated using the forward scattering of the photoelectrons emitted from the innermost nitrogen atom [3.34]. The separated spectra from the two different nitrogen atoms are shown in Fig. 3.35. The shake-up spectra are significantly different, which further demonstrates the local character of the core ionization process.

It is interesting to compare the spectrum from the outer nitrogen atom with the C 1$s$ shake-up spectrum from adsorbed CO. This can be seen by using the $Z+1$ approximation of the core ionized final states. Both lead to a final state similar to an adsorbed NO molecule bonding with the nitrogen end towards the

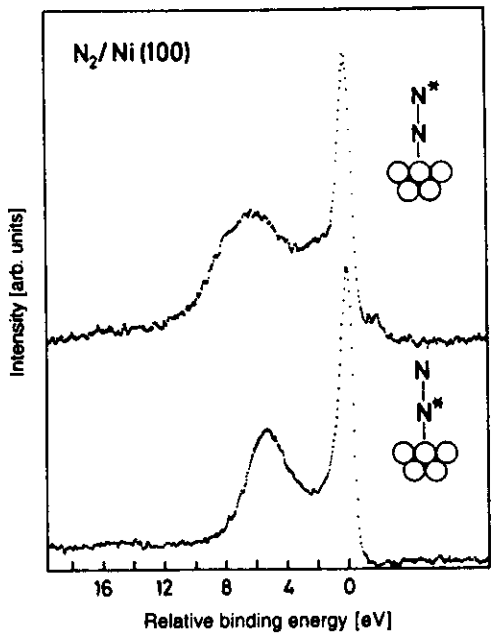


Fig. 3.35. Separated N 1$s$ spectra for $N_2$ on Ni(100) in a $c(2\times2)$ structure. The spectra are aligned according to the main line positions. The separation was carried out by measuring the N 1$s$ spectra at two different angles with respect to the surface normal, 5° and 35°, respectively, and making two subtractions. The intensity from the inner nitrogen atom is strongly enhanced for emission angles along the surface normal

surface. Figure 3.36 compares the C 1*s* spectrum in CO and the N 1*s* in $N_2$ from the outer nitrogen atom [3.34]. There is a clear similarity between the main shake-up features in the two spectra which show the same three-peak structure. Only the third state appears at slightly different energies. However, the intensities of the various shake-up states in the two spectra are quite different. The C 1*s* satellites are generally about a factor of two less intense.

The three shake-up states have different origins [3.34]. The first one is related to excitations between adsorbate-substrate bonding to antibonding states, the second peak involves higher and more extended adsorbate states derived from the molecular np Rydberg states, and the third is derived from an internal molecular excitation which is also seen in the free molecule.

In Sect. 3.4.1, the interaction of the CO $2\pi^*$ orbital with the Ni substrate was described [3.11, 31]. This interaction leads to splitting of the $2\pi^*$ mainfold into bonding ($2\pi_b$) and antibonding ($2\pi_a$) states with the Ni 3*d* states. Furthermore, these states are strongly perturbed by the presence of the core hole which is illustrated in Fig. 3.8. The core-hole and the charge transfer in the metallic screening process change the character of the $2\pi_b$ states. It can therefore be anticipated that the $2\pi_b$ states become strongly involved in the various shake-up excitations. The first peak at around 2 eV, Fig. 3.36, can be interpreted as transitions between the $2\pi_b$–$2\pi_a$ states in the final-state molecule, as depicted in Fig. 3.8b.

We can now describe the difference in the N 1*s* spectra for the two different nitrogen atoms in Fig. 3.35 [3.34]. As was shown in Sect. 3.4.2, the final state

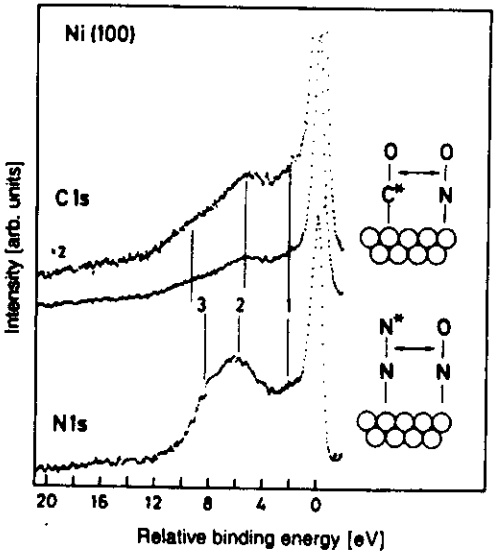


**Fig. 3.36.** C 1*s* spectrum from CO adsorbed on Ni(100) in a $c(2\times2)$ structure and N1*s* spectrum from the outer nitrogen atom of $N_2$ on Ni(100). The spectra have been recorded at 80 K. The spectra are aligned according to the main line positions



NO-like molecule interacts very weakly with the substrate in the orientation with the oxygen end down. The weak adsorbate-substrate interaction leads to negligible splitting of the $2\pi^*$ level, which is why no satellite associated with the $2\pi_b$–$2\pi_a$ transition is observed at 2 eV.

The strong satellites at around 5–6 eV which are seen in all spectra are assigned to transitions of the $2\pi_b$ screening states into 3*s*, 3*p* and 4*p* derived states [3.31]. These Rydberg derived states have recently been observed in XA spectra of adsorbed CO and $N_2$ on Ni [3.127]. The Rydberg orbitals observed in the free molecule survive upon chemisorption and form new hybridized adsorbate-substrate states. Similar valence-electron excitation energies have been observed in the analogue NO/Ni. These spectra show a broad electronic transition centered around 5.5 eV [3.128]. This peak has been assigned to transitions from the $2\pi^*$ level into Rydberg states. However, recent INDO-CI calculations on $Mo(CO)_6$ show that the excitation of the carbonyl complex is split into a triplet and a singlet parent coupled state of the $2\pi_b$ to $2\pi_a$ transition due to exchange interaction of the open shells [3.129]. The singlet state appears at 6 eV above the main line. It is therefore possible that some of the intensity in this region for the adsorbate has this origin and may overlap with the Rydberg transitions.

The third peak in the shake-up spectra nearly coincides in energy with the first C 1*s* and N 1*s* shake-up states in free CO and $N_2$. This transition has been assigned to a $1\pi$–$2\pi^*$ excitation related to the intramolecular relaxation [3.89].

In Figs. 3.37 and 38, we compare the C 1*s* and O 1*s* spectra for CO chemisorbed on Ni(100), Cu(100) and Ag(110) [3.126]. The spectra show the so-called *giant satellites* in the case of adsorption on Cu and Ag. The main line in the C 1*s* spectrum for CO on Ag(110) is only a tiny structure preceding the totally dominating satellites. A lot of fine structure is observed, resulting in rather complicated spectra. We will concentrate on the features in C 1*s* spectra in relation to the discussion of CO and $N_2$ on Ni; a more detailed description has been given by *Tillborg* et al. [3.126].

The $2\pi_b$ states for NO are due to the hybridization with the metal *d*-states. In Ni, the *d*-band is not completely filled and the $2\pi_b$ states are found around 1 eV below the Fermi level. In Cu and Ag, the *d*-band is filled and positioned about 2 eV and 4 eV below the Fermi level. It can therefore be anticipated that the $2\pi_b$ states shift downwards in energy when NO is chemisorbed on Cu and Ag. The $2\pi_a$ states as probed by XAS, are located just above the Fermi level on all the substrates [3.30]. The $2\pi_b$–$2\pi_a$ shake-up transition energy will therefore increase going from Ni to Cu to Ag. This is observed in the C 1*s* shake-up spectrum in Fig. 3.37 where the corresponding excitation energy goes from 2 eV in Ni to 3 eV in Cu and 4.2 eV in Ag. Furthermore, the intensities of the shake-up transitions increase dramatically as the *d*-band is shifted to higher energies. Recent studies for CO on Au(110) confirm this picture [3.73]. The *d*-band in Au is located between the *d*-bands in Cu and Ag. The shake-up spectrum has an appearance which places it between CO on Cu and CO on Ag both in terms of energies and intensities.

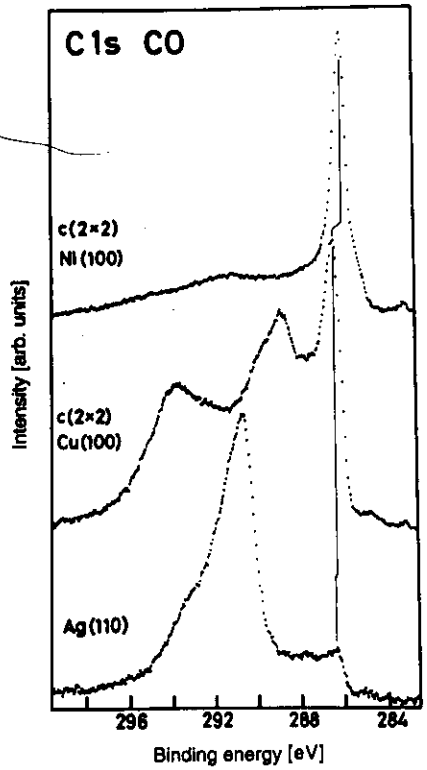


Fig. 3.37. C 1s region from CO adsorbed on Ni(100), Cu(100) and Ag(110). For the two former substrates, the overlayer structures involve purely on top adsorption sites. For CO/Ag(110) the adsorption geometry and site is not known

The satellite intensity is related to the difference in electronic structure between the initial and lowest energy final states. A large shake-up intensity indicates that the lowest final state deviates strongly from (is close to orthogonal to) the Koopmans' state. For adsorbed CO, it can be argued that the shake-up intensity should relate to the population of the molecular $2\pi_b$ orbital in the ground state (adsorbed CO without core-hole). This orbital is populated by approximately one electron in the core-ionized molecule, because of charge transfer screening from the metal (Sect. 3.4.1). The relative change between the initial and final states, and thus the satellite intensity, is larger if the ground-state population is low. This indicates that the ground state CO-$2\pi^*$ population in the $2\pi_b$ state is lower for CO on Cu and Ag than on Ni, which can be expected because of smaller interaction strengths.

The same arguments can be used in the NO-like final states for CO and $N_2$ on Ni(100) in Fig. 3.35. The fact that the shake-up intensity is lower in the C 1*s* spectrum in CO than in the N 1*s* spectrum in $N_2$ may be taken as a sign of a larger occupation of the $2\pi^*$ orbital in CO. Due to the difference in electronega-



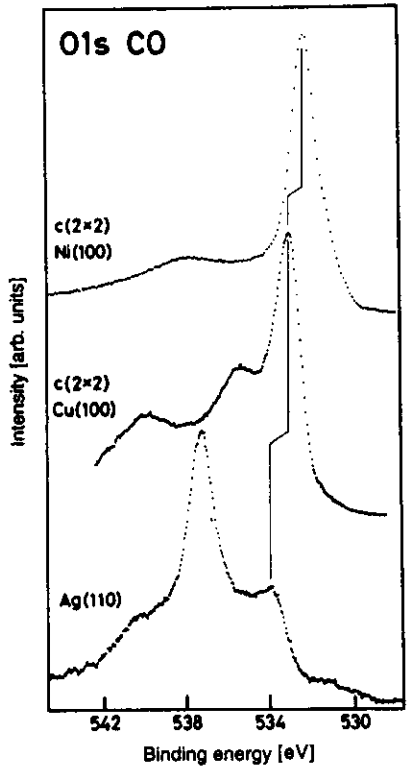


Fig. 3.38. O 1s region from CO adsorbed on Ni(100), Cu(100) and Ag(110). For the two former substrates, the overlayer structures involve purely on top adsorption sites. For CO/Ag(110) the adsorption geometry and site is not known

tivity between C and O the $2\pi^*$ orbital is more localized on the carbon atom allowing for a larger overlap with metal states in the substrate than for $N_2$.

In order to make a correct estimation of the satellite intensity, relative to the main line, it is necessary to include the complete shake-off continuum. The extended satellite spectra for the C 1*s* lines from CO adsorbed on Ni(100) (lower) and Cu(100) (upper) are depicted in Fig. 3.39 [3.126]. It is seen that a substantial part of the whole intensity extends up to 70 eV above the main lines. Similar shake-off intensities are observed in the O 1*s* spectrum from CO/Ni(100) and in $N_2$/Ni(100). Two structures are clearly seen in the CO/Cu(100) spectrum at about 23 and 35 eV above the main line. A broad feature is centered at 35 eV in the spectrum from CO/Ni(100). States at these energies have been observed in the C1*s* spectrum from $Cr(CO)_6$. The assignment of these states is not straightforward but can be regarded as shake-off resonances, as discussed in [3.31]. The C1*s* main line/total spectrum intensity ratios are estimated to be 0.12 and 0.29 for CO on Cu(100) and Ni(100), respectively. These ratios may be compared to the corresponding ratio of 0.67 for the free molecule. The observation of satellite

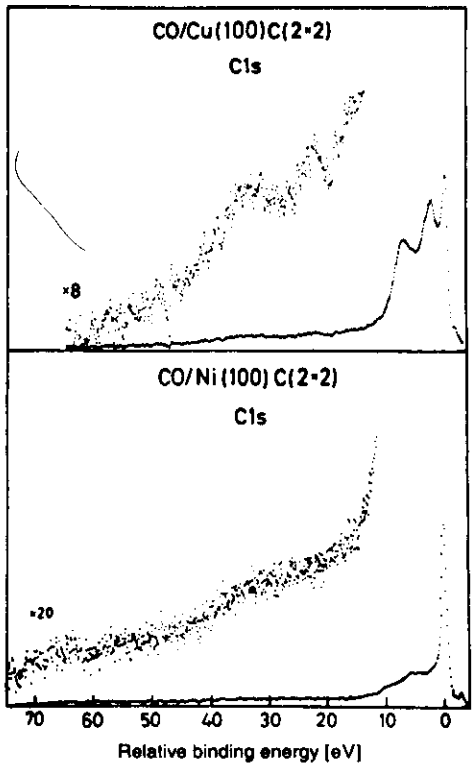


**Fig. 3.39.** Extended C 1s shake-up and shake-off spectra from CO adsorbed in a $c(2 \times 2)$ structure on Ni(100) and Cu(100). The spectra are aligned according to the main line positions and normalized to give the same main line peak height. Note the different enlargement of the two shake-off continua

intensity up to more than 70 eV above the main line is important not only in the use of core-level photoemission for quantitative analysis but also for the fundamental understanding of the photoionization process in adsorbates.

*Acknowledgements.* We gratefully acknowledge the people involved in the various projects on which this chapter is based, especially the former students Helena Tillborg, Anders Sandell, Olle Björneholm, Anders Stenborg and Erik Zdansky and the present students Bo Hernnäs and Peter Bennich. We also acknowledge the many fruitful discussions with Svante Svensson, Hans Ågren, Sten Lunell, Ulrik Gelius, Jesper Andersen, Ralf Nyholm, Börje Johansson, Richard Palmer, Jo Stöhr and Paul Brühwiler. The technical assistance of Jan-Olof Forsell has been invaluable.

## References

3.1 K. Siegbahn, C. Nordling, G. Johansson, J. Hedman, P.F. Heden, K. Hamrin, U. Gelius, T. Bergmark, L.O. Werme, R. Manne, Y. Baer: *ESCA Applied to Free Molecules* (North-Holland, Amsterdam 1969)



3.2 C.S. Fadley: *Electron Spectroscopy: Theory, Techniques and Applications* (Academic Press, New York 1978) Vol. 2
3.3 B. Feuerbacher, B. Fitton, R.F. Willis (eds.): *Photoemission and the Electronic Properties of Surfaces* (Wiley, New York 1978)
3.4 D. Menzel: In *Chemistry and Physics of Solid Surfaces*, ed. by R. Vanselow. (CRC Press, Boca Raton, FL 1979) Vol. II, p. 277
3.5 H. Siegbahn, L. Karlsson: In *Corpuscles and Radiation in Matter*, ed. by W. Mehlhorn, Handbuch der Physik, Vol. 31 (Springer, Berlin, Heidelberg 1982), vol. XXXI
3.6 M. Scheffler, A.M. Bradshaw: In *The Chemical Physics of Solid Surfaces and Heterogenous Catalysis*, ed. by D.A. King, D.P. Woodruff, (Elsevier, Oxford 1983) Vol. 2, p. 165
3.7 E.W. Plummer, C.T. Chen, W.K. Ford, W. Eberhardt, R.P. Messner, H. J. Freund: Surf. Sci. **158**, 58 (1985)
3.8 W.F. Egelhoff: Surf. Sci. Reps. **6**, 253 (1986)
3.9 N. Mårtensson, A. Nilsson: J. Elec. Spec. and Relat. Phenom. **52**, 1 (1990)
3.10 J. Stöhr: *NEXAFS Spectroscopy* Springer Ser. Surf. Sci., Vol. 25 (Springer, Berlin, Heidelberg 1992)
3.11 A. Nilsson, E. Zdansky, H. Tillborg, O. Björneholm, N. Mårtensson, J.N. Andersen, R. Nyholm: Chem. Phys. Lett. **197**, 12 (1992)
3.12 J.C. Fuggle: In *Electron Spectroscopy IV* ed. by C.R. Brundle, A.D. Baker, (Academic London 1981) p. 85
3.13 O. Björneholm, A. Sandell, A. Nilsson, N. Mårtensson, J.N. Andersen: Physica Scripta **T41**, 217 (1992)
3.14 J. Nordgren, N. Wassdahl: Physica Scripta T **31**, 103 (1990)
3.15 N. Wassdahl, A. Nilsson, T. Wiell, H. Tillborg, L.-C. Duda, J.H. Guo, N. Mårtensson, J. Nordgren, J.N. Andersen, R. Nyholm, Phys. Rev. Lett. **69**, 812 (1992)
3.16 C.S. Fadley, In *Synchrotron Radiation Research: Advances in Surface and Interface Science*, ed. by R.Z. Bachrach (Plenum, New York 1992) p. 421
3.17 A. Nilsson, A. Stenborg, O. Björneholm, N. Mårtensson, J.N. Andersen, C. Wigren (to be published)
3.18 N. Mårtensson, A. Stenborg, O. Björneholm, A. Nilsson, J.N. Andersen: Phys. Rev. Lett. **60**, 1731 (1988)
3.19 A. Nilsson, B. Eriksson, N. Mårtensson, J.N. Andersen, J. Onsgaard: Phys. Rev. B **38**, 10357 (1988)
3.20 T.A. Carlsson: Phys. Rev. **156**, 142 (1967)
3.21 N. Mårtensson, S. Svensson, U. Gelius: J. Phys. B **20**, 6243 (1987)
3.22 S. Svensson, B. Eriksson, N. Mårtensson, U. Gelius, G. Wendin: J. Elec. Spec. and Relat. Phenom. **47**, 327 (1988)
3.23 L.J. Saethre, T.D. Thomas, L. Ungier: J. Elec. Spec. and Relat. Phenom. **33**, 381 (1984)
3.24 L. Asplund, U. Gelius, S. Hedman, K. Helenelund, K. Siegbahn, P.E.M. Siegbahn: J. Phys. B **18**, 1569 (1985)
3.25 U. Gelius, S. Svensson, H. Siegbahn, E. Basilier, Å. Faxälv, K. Siegbahn: Chem. Phys. Lett. **28**, 1 (1974)
3.26 A. Nilsson, N. Mårtensson: Solid State Commun. **70**, 923 (1989)
3.27 A. Nilsson, N. Mårtensson: Phys. Rev. Lett. **63**, 1483 (1989)
3.28 N. Mårtensson: P. Baltzer, P.A. Brühwiler, J. Forsell, A. Nilsson, A. Stenborg, B. Wannberg, J. Elec. Spec. and Relat. Phenom., In press
3.29 P. Baltzer, L. Karlsson, M. Lundqvist, B. Wannberg: Rev. Sci. Instrum. **64**, 2174 (1993)
3.30 J.N. Andersen, O. Björneholm, A. Sandell, R. Nyholm, J. Forsell, L. Thånell, A. Nilsson, N. Mårtensson: Synchrotron Radiation News **4**, 15 (1991)
3.31 A. Nilsson, N. Mårtensson: Phys. Rev. B **40**, 10249 (1989)
3.32 U. Gelius, L. Asplund, E. Basilier, S. Hedman, K. Helenelund, K. Siegbahn, Nucl. Instrum. and Meth. **B 1**, 85 (1984)
3.33 B. Johansson, N. Mårtensson: Phys. Rev. B **21**, 4427 (1980)
3.34 A. Nilsson, H. Tillborg, N. Mårtensson, Phys. Rev. Lett. **67**, 1015 (1991)

3.35 W.F. Egelhoff Jr.: Surf. Sci 141, L324 (1984)
3.36 H. Antonsson, A. Nilsson, N. Mårtensson, I. Panas, P.E.M. Siegbahn: J. Elec. Spec. and Relat. Phenom. 54/55, 601 (1990)
3.37 A. Nilsson, H. Antonsson, A. Sandell, N. Mårtensson: In *The Structure of Surfaces III* Springer Ser. Surf, Sci, Vol. 24 (Springer, Berlin, Heidelberg 1991) p. 467
3.38 H. Basch: J. Elec. Spec. and Relat. Phenom. 5, 463 (1974)
3.39 U. Gelius: J. Elec. Spec. and Relat. Phenom. 5, 985 (1974)
3.40 A. Nilsson, R.E. Palmer, H. Tillborg, B. Hernnäs, R.J. Guest, N. Mårtensson: Phys. Rev. Lett. 68, 982 (1992)
3.41 M. Larsson, P. Baltzer, S. Svensson, B. Wannberg, N. Mårtensson, A. Naves de Brito, N. Correia, M.P. Keane, M. Carlsson-Göthe, L. Karlsson: J. Phys. B 23, 1175 (1990)
3.42 R.M. Lambert, M.E. Bridge: In *The Chemical Physics of Solid Surfaces and Heterogeneous Catalysis*, ed. by D.A. King, D.P. Woodruff, (Elsevier, New York 1984), Vol. 3B
3.43 A. Sandell, A. Nilsson, N. Mårtensson: Surf. Sci. 251/252, 971 (1991)
3.44 P. Uvdal, P.A. Karlsson, C. Nyberg, S. Andersson, N.V. Richardsson: Surf. Sci. 202, 167 (1988)
3.45 H. Tillborg, A. Nilsson, N. Mårtensson: Surf. Sci. 273, 47 (1992)
3.46 L. Westerlund, L. Jönsson, S. Andersson: Surf. Sci. 199, 109 (1988)
3.47 P.R. Norton, J.W. Goodale, E.B. Selkirk: Surf. Sci. 83, 189 (1979)
3.48 H. Tillborg, A. Nilsson, N. Mårtensson: To be published
3.49 A. Sandell, A. Nilsson, N. Mårtensson, Surf. Sci. 241, L1 (1991)
3.50 J. Stöhr, R. Jaeger: Phys. Rev. B 26, 411 (1982)
3.51 J.L. Gland, B.A. Sexton, G.B. Fisher: Surf. Sci. 95, 587 (1980)
3.52 W. Wurth, J. Stöhr, P. Feulner, X. Pan, K.R. Bauchspiess, Y. Baba, E. Hudel, G. Rocker, D. Menzel: Phys. Rev. Lett. 65, 2426 (1990)
3.53 R.J. Guest, O. Björneholm, B. Hernnäs, A. Nilsson, R.E. Palmer, P. Bennich, N. Mårtensson: Surf. Sci. 278, 239 (1992)
3.54 G. Odörfer, R. Jaeger, G. Illing, H. Kuhlenbeck, H.J. Freund: Surf. Sci. 233, 44 (1990)
3.55 R.E. Palmer, P.J. Rous: Rev. Mod. Phys. 64, 383 (1992)
3.56 R.J. Guest, A. Nilsson, O. Björneholm, B. Hernnäs, A. Sandell, R.E. Palmer, N. Mårtensson: Surf. Sci. 269/270, 432 (1992)
3.57 H. Tillborg, A. Nilsson, B. Hernnäs, N. Mårtensson, R.E. Palmer: Surf. Sci. 295, 1 (1993)
3.58 T.-C. Chiang, G. Kaindl, T. Mandel: Phys. Rev. B 33, 695 (1986)
3.59 G. Kaindl, T.C. Chiang, D.E. Eastman, F.J. Himpsel: Phys. Rev. Lett. 45, 1808 (1980)
3.60 K. Jacobi, H.H. Rotermund: Surf. Sci. 116, 435 (1982)
3.61 T. Mandel, M. Domke, G. Kaindl, C. Laubschat, M. Prietsch, U. Middelman, K. Horn: Surf. Sci. 162, 453 (1985)
3.62 K. Jacobi: Phys. Rev. B 38, 6291 (1988)
3.63 D. Nordfors, H. Ågren, K.V. Mikkelsen: Chem. Phys. Lett. 164, 173 (1992)
3.64 B. Johansson, N. Mårtensson: Helvetica Physica Acta 56, 405 (1983)
3.65 P.H. Citrin, G.K. Wertheim: Phys. Rev. B 27, 3176 (1983)
3.66 D. Spanjard, C. Guillot, M.C. Desjonquéres: Surf. Sci. Rep. 5, 1 (1985)
3.67 A. Flodström, R. Nyholm, B. Johansson: In *Synchrotron Radiation Research: Advances in Surface and Interface Science*, ed. by R.Z. Bachrach. (Plenum, New York 1992) Vol. 1, p. 199
3.68 W.F. Egelhoff Jr.: Crit. Rev. of Solid State and Mathematical Sci. 16, 213 (1990)
3.69 N. Mårtensson, H.B. Saalfeld, H. Kuhlenbeck, M. Nuemann: Phys. Rev. B 39, 8181 (1989)
3.70 D. Tománek, V. Kumar, S. Holloway, K. H. Bennemann: Solid State Commun. 41, 273 (1982)
3.71 A. Rosengren, B. Johansson: Phys. Rev. B 22, 3706 (1980)
3.72 A. Nilsson, O. Björneholm, A. Sandell, P. Bennich, B. Hernnäs, C. Puglia, N. Mårtensson: To be published
3.73 A. Sandell, P. Bennich, A. Nilsson, B. Hernnäs, O. Björneholm, N. Mårtensson: Surf. Sci., 310, 16 (1994)
3.74 O. Björneholm, A. Nilsson, H. Tillborg, P. Bennich, A. Sandell, B. Hernnäs, C. Puglia, N. Mårtensson: Surf. Sci., In press





3.75 M. Tüshaus, E. Schweizer, P. Hollins, A.M. Bradshaw: J Elec. Spec. and Relat. Phenom. 44 305 (1987)
3.76 M.O. Krause, J.H. Oliver: J. Phys. and Chem. Ref. Data 8, 329 (1979)
3.77 S. Svensson, N. Mårtensson, E. Basilier, P.-Å. Malmquist, U. Gelius, K. Siegbahn: Physic. Scripta 14, 141 (1976)
3.78 G. Wendin, M. Ohno: Physica Scripta 14, 148 (1976)
3.79 S. Doniach, M. Sunjic: J. Phys. C 3, 285 (1970)
3.80 S. Tougaard: Phys. Rev. B 34, 6779 (1986)
3.81 H. Wiedemann: *Particle Accelerator Physics* (Springer, Berlin, Heidelberg 1993)
3.82 M. Bader, C. Ocal, B. Hillert, J. Haase, A.M. Bradshaw: Phys. Rev. B 35, 5900 (1987)
3.83 L. Wenzel, D. Arvanitis, W. Daum, H.H. Rotermund, J. Stöhr, K. Baberschke, H. Ibach: Phys Rev. B 36, 7689 (1987)
3.84 J. Stöhr, R. Jaeger, T. Kendelewicz: Phys. Rev. Lett. 49, 142 (1982)
3.85 W. Daum, S. Lehwald, H. Ibach: Surf. Sci. 178, 528 (1986)
3.86 M. Rocca, S. Lehwald, H. Ibach, T.S. Rahman: Phys. Rev. B 35, 9510 (1987)
3.87 M. Rocca, S. Lehwald, H. Ibach: Surf. Sci. 163, L738 (1985)
3.88 N. Mårtensson, A. Nilsson: Surf Sci. 211/212, 303 (1989)
3.89 J. Schirmer, G. Angonoa, S. Svensson, D. Nordfors, U. Gelius: J. Phys. B 20, 6031 (1987)
3.90 A.P. Hitchcock, C.E. Brion: J. Elec. Spec. and Relat. Phenom. 18, 1 (1980)
3.91 A. Nilsson, N. Mårtensson, S. Svensson, L. Karlsson, D. Nordfors, U. Gelius, H. Ågren J. Chem. Phys. 96, 8770 (1992)
3.92 S. Andersson, Solid State Commun. 21, 75 (1977)
3.93 R. Berndt, J.P. Toennies, C. Wöll: J. Elec. Spec. 44, 183 (1987)
3.94 N.V. Richardson, A.M. Bradshaw: Surf. Sci. 88, 255 (1979)
3.95 A.M. Lahee, J.P. Toennies, C. Wöll: Surf. Sci. 177, 371 (1986)
3.96 G. Doyen, G. Ertl: Surf. Sci. 69, 157 (1977)
3.97 R.L. Martin, D.A. Shirley: Phys. Rev. A 13, 1475 (1976)
3.98 R. Arneberg, J. Müller, R. Manne: Chemical Physics 64, 249 (1982)
3.99 T. Åberg: Ann. Acad. Sci. Fennicae (Ser. A) IV, 308 (1969)
3.100 R. Manne, T. Åberg: Chem. Phys. Lett. 7, 282 (1970)
3.101 B.I. Lundqvist: Phys. Kondens. Materie 9, 236 (1969)
3.102 A. Sandell, A. Nilsson, P. Bennich, N. Mårtensson: Phys. Rev. Lett. 72, 2604 (1994)
3.103 A. Hoffman, G.L. Nyberg, J. Liesegang: Phys. Rev. B 45, 5679 (1992)
3.104 A. Nilsson, O. Björneholm, A. Sandell, B. Hernnäs, N. Mårtensson: Surf. Sci. 293, L835 (1993)
3.105 N. Mårtensson, R. Nyholm, B. Johansson: Phys. Rev, B 29 (1984)
3.106 C.W. Bates, G.K. Wertheim, D.N.E. Buchanan, Phys. Lett. A 72, 178 (1979)
3.107 R.A. Pollak, L. Ley, F.R. McFeely, S.P. Kowalczyk, D.A. Shirley: J. Elec. Spec. and Relat. Phenom. 3, 381 (1974)
3.108 D. Lovric, B. Gumhalter: Phys. Rev. B 38, 10323 (1988)
3.109 A. Nilsson, N. Mårtensson: Chem. Phys. Lett. 182, 147 (1991)
3.110 E. Zdansky, A. Nilsson, H. Tillborg, O. Björneholm, N. Mårtensson, J.N. Andersen, R. Nyholm: Phys. Rev. B 48, 2632 (1993)
3.111 H. Tillborg, A. Nilsson, T. Wiell, N. Wassdahl, N. Mårtensson, J. Nordgren: Phys. Rev. B 47, 16464 (1993)
3.112 C.E. Moore: *Atomic Energy Levels* (National Bureau of Standards, Washington, DC 1949 Vol. 1
3.113 C.W. Bauschlichter: J. Chem. and Phys. 84, 250 (1986)
3.114 A. Bosch, H. Feil, G.A. Sawatzky, N. Mårtensson, Solid State Commun. 41, 355 (1982)
3.115 J.C. Fuggle, U.E, D. Menzel, K. Wandelt, C.R. Brundle: Solid State Commun. 27, 65 (1978)
3.116 E. Umbach: Surf. Sci. 117, 482 (1982)
3.117 K. Schönhammer, O. Gunnarsson: Solid State Commun. 23, 691 (1977)
3.118 O. Gunnarsson, K. Schönhammer: Phys. Rev. Lett. 41, 1608 (1978)
3.119 P.S. Bagus, M. Seel: Phys. Rev. B 23, 2065 (1981)

3.120 H.-J. Freund, E.W. Plummer: Phys. Rev. B **23**, 4859 (1981)
3.121 R.P. Messmer, S.H. Lamson, D.R. Salahub: Phys. Rev. B **25**, 3576 (1982)
3.122 H.J. Freund, F. Greuter, D. Heskett, E.W. Plummer, Phys. Rev. B **28**, 1727 (1983)
3.123 E. Umbach: Solid State Commun. **51**, 365 (1984)
3.124 H.-J. Freund, R.P. Messmer, C.M. Kao, E.W. Plummer: Phys. Rev. B **31**, 4848 (1985)
3.125 D. Lovric, B. Gumhalter, K. Wandelt: Surf. Sci. **278**, 1 (1992)
3.126 H. Tillborg, A. Nilsson, N. Mårtensson: J. Elec. Spec. and Relat. Phenom. **62**, 73 (1993)
3.127 O. Björneholm, A. Nilsson, E. Zdansky, A. Sandell, H. Tillborg, B. Hernnäs, N. Mårtensson, J.N. Andersen: Phys. Rev. B **47**, 2308 (1993)
3.128 P. Avouris, N.J. Dinardo, J.E. Demuth: J. Chem. and Phys. **80**, 491 (1984)
3.129 J. Burstad, C. Engkvist, S. Lunell, H. Tillborg, A. Nilsson, S. Osborne, N. Mårtensson, S. Svensson: Chem. Phys. **179**, 303 (1994)
3.130 O. Björneholm, A. Nilsson, E. Zdansky, A. Sandell, H. Tillborg, N. Mårtensson, J.N. Andersen, R. Nyholm: Phys. Rev. B **46**, 10353 (1992)